Report

Cell Reports

The Mitochondrial Calcium Uniporter Matches Energetic Supply with Cardiac Workload during Stress and Modulates Permeability Transition

Graphical Abstract

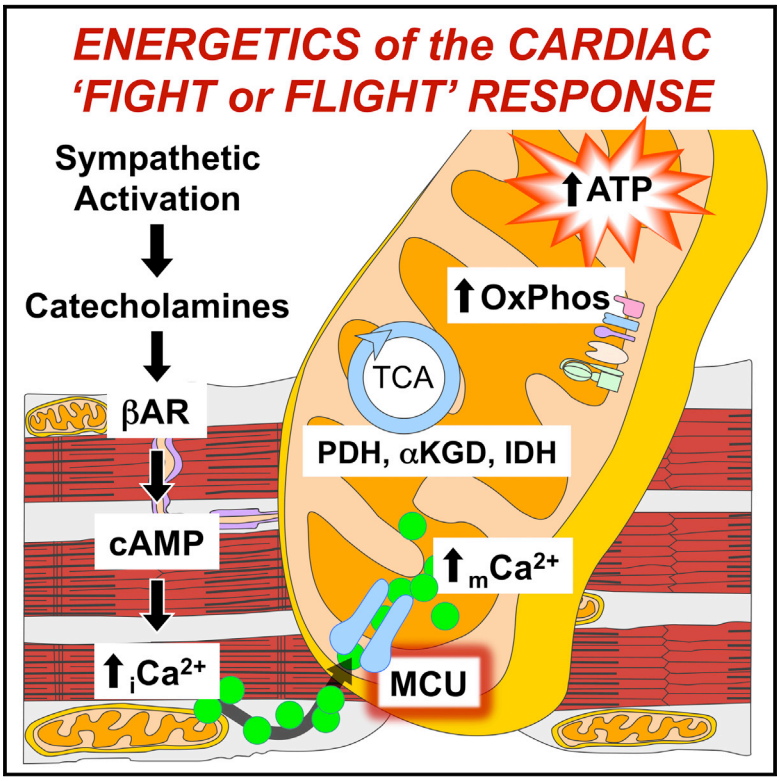

Highlights

- The MCU is dispensable for baseline homeostatic cardiac function
- Deletion of *Mcu* protects against myocardial IR injury by reducing MPTP activation
- The MCU is required to match energetics with contractile demand during stress
- A slow MCU-independent uptake mechanism may maintain basal matrix $_{m}Ca^{2+}$ content

Authors

Timothy S. Luongo, Jonathan P. Lambert, Ancai Yuan, ..., Joseph Y. Cheung, Muniswamy Madesh, John W. Elrod

Correspondence

elrod@temple.edu

In Brief

Luongo et al. show, using a conditional knockout mouse model, that the mitochondrial Ca^{2+} uniporter (MCU), although dispensable for homeostatic function, is necessary for the cardiac "fight-or-flight" contractile response and a significant contributor to mitochondrial permeability transition during ischemia-reperfusion injury.

Luongo et al., 2015, Cell Reports *12*, 1–12
July 14, 2015
http://dx.doi.org/10.1016/j.celrep.2015.06.017

CellPress

Please cite this article in press as: Luongo et al., The Mitochondrial Calcium Uniporter Matches Energetic Supply with Cardiac Workload during Stress and Modulates Permeability Transition, Cell Reports (2015), http://dx.doi.org/10.1016/j.celrep.2015.06.017

Cell Reports
Report

The Mitochondrial Calcium Uniporter Matches Energetic Supply with Cardiac Workload during Stress and Modulates Permeability Transition

Timothy S. Luongo,[1] Jonathan P. Lambert,[1] Ancai Yuan,[1] Xueqian Zhang,[1] Polina Gross,[3] Jianliang Song,[1] Santhanam Shanmughapriya,[1] Erhe Gao,[1] Mohit Jain,[2] Steven R. Houser,[3] Walter J. Koch,[1] Joseph Y. Cheung,[1] Muniswamy Madesh,[1] and John W. Elrod[1,*]

[1]Center for Translational Medicine, Department of Pharmacology, Temple University School of Medicine, Philadelphia, PA 19140, USA
[2]Department of Pharmacology, University of California San Diego, La Jolla, CA 92093, USA
[3]Center for Cardiovascular Research, Department of Physiology, Temple University School of Medicine, Philadelphia, PA 19140, USA
*Correspondence: elrod@temple.edu
http://dx.doi.org/10.1016/j.celrep.2015.06.017

SUMMARY

Cardiac contractility is mediated by a variable flux in intracellular calcium (Ca^{2+}), thought to be integrated into mitochondria via the mitochondrial calcium uniporter (MCU) channel to match energetic demand. Here, we examine a conditional, cardiomyocyte-specific, mutant mouse lacking *Mcu*, the pore-forming subunit of the MCU channel, in adulthood. *Mcu*$^{-/-}$ mice display no overt baseline phenotype and are protected against $_{m}Ca^{2+}$ overload in an in vivo myocardial ischemia-reperfusion injury model by preventing the activation of the mitochondrial permeability transition pore, decreasing infarct size, and preserving cardiac function. In addition, we find that *Mcu*$^{-/-}$ mice lack contractile responsiveness to acute β-adrenergic receptor stimulation and in parallel are unable to activate mitochondrial dehydrogenases and display reduced bioenergetic reserve capacity. These results support the hypothesis that MCU may be dispensable for homeostatic cardiac function but required to modulate Ca^{2+}-dependent metabolism during acute stress.

INTRODUCTION

The cardiomyocyte is unique in that a large and variable flux of intracellular calcium ($_{i}Ca^{+2}$) must occur to mediate and regulate contraction. Thus, a complex system has evolved to regulate $_{i}Ca^{2+}$ transport to maintain homeostatic conditions (Bers, 2008). Numerous genetic components have been shown to mediate the passage of $_{i}Ca^{2+}$ across the sarcolemma and sarcoplasmic reticulum (SR), and, while great strides have been made toward understanding the temporal and spatial relationship of Ca^{2+} in regards to excitation-contraction (EC) coupling, our understanding of other sub-cellular Ca^{2+} domains, including the components of mitochondria Ca^{2+} ($_{m}Ca^{2+}$) exchange, remains elementary.

The dynamic Ca^{2+} environment of the heart requires that cardiac mitochondria possess an exchange system capable of dealing with the variable changes in Ca^{2+} load. Ca^{2+} enters the mitochondrial matrix via the mitochondria calcium uniporter (MCU). The MCU is an inward rectifying, low-affinity, high-capacity channel whose uptake is mediated by mitochondrial membrane potential ($\Delta\psi$ = approximately −180 mV) generated by the electron transport chain (ETC) (Kirichok et al., 2004). The recent identification of the gene encoding the channel-forming portion of the uniporter, formerly named *CCDC109A* now known as *MCU*, has opened the field to genetic gain- and loss-of-function studies to determine experimentally the true role of $_{m}Ca^{2+}$ signaling in the regulation of numerous proposed cellular processes (Baughman et al., 2011; De Stefani et al., 2011). To date, multiple reports have confirmed MCU as being required for acute $_{m}Ca^{2+}$ influx into the matrix. However, numerous outstanding questions remain in regards to the molecular regulation of the MCU and the physiological function of $_{m}Ca^{2+}$, particularly in excitable cells such as cardiomyocytes.

The high metabolic demand of contractility makes it essential that an efficient and tightly controlled system be in place to regulate energy production. Oxidative Phosphorylation (OxPhos) is the largest contributor to myocardial metabolism and as such the mitochondria represents a central control point to ensure that energy demands are met. Simultaneous measurements of $_{m}Ca^{2+}$ and NADH have correlated increased $_{m}Ca^{2+}$ load with increased oxidative phosphorylation and ATP production (Brandes and Bers, 2002; Unitt et al., 1989). Thus, Ca^{2+} is proposed to be the link between EC coupling (ECC) and OxPhos and has been shown to modulate mitochondrial metabolism through numerous mechanisms including the activation of Ca^{2+}-dependent dehydrogenases and modulation of ETC complexes (Glancy and Balaban, 2012).

In contrast to the aforementioned pro-survival metabolic signaling, numerous studies have implicated $_{m}Ca^{2+}$ overload in the activation of apoptosis and necrosis (Rasola and Bernardi, 2011). $_{m}Ca^{2+}$ is known to cause outer-mitochondrial membrane (OMM) permeability prompting the release of apoptogens. Ca^{2+} is also thought to be the major priming event in the opening of the

Please cite this article in press as: Luongo et al., The Mitochondrial Calcium Uniporter Matches Energetic Supply with Cardiac Workload during Stress and Modulates Permeability Transition, Cell Reports (2015), http://dx.doi.org/10.1016/j.celrep.2015.06.017

mitochondrial permeability transition pore (MPTP) causing the collapse of $\Delta\psi$ and loss of ATP production resulting in necrotic cell death. This mechanism of cellular demise is believed to significantly contribute to the initiation and progression of myocardial infarction and heart failure (Foo et al., 2005). In addition, it has been speculated that mitochondria in close contact to the sarcoplasmic reticulum (SR) may buffer $_{i}Ca^{2+}$ cycling and thereby play a direct role in modulating EC coupling, providing yet another layer of potential regulation (Drago et al., 2012; Rizzuto et al., 1998).

To begin to unravel how $_{m}Ca^{2+}$ signaling modulates in vivo physiology, a group at the NHLBI recently generated a *Mcu* gene-trap mouse (Pan et al., 2013). As expected, mitochondria isolated from this global *Mcu*-null mouse failed to take up Ca^{2+}. However, while they did find alterations in some aspects of skeletal muscle work capacity, they did not find a significant cardiac phenotype. Particularly intriguing, they found no change in myocardial infarct size in an ex vivo global ischemia model even though in vitro indices of MPTP opening appeared to be completely absent. These surprising results have spurred the field to question the true role of $_{m}Ca^{2+}$ signaling in the normal and diseased heart.

To advance our understanding of $_{m}Ca^{2+}$ uptake in the heart, in collaboration with the Molkentin lab, we generated a conditional, loss-of-function mouse model ($Mcu^{fl/fl}$) and coupled with a tamoxifen-inducible, cardiomyocyte-specific Cre recombinase transgenic line, deleted *Mcu* in adulthood (Kwong et al., 2015 [this issue of *Cell Reports*]). Here, we report that loss of *Mcu* ablates $_{m}Ca^{2+}$ uptake and activity (I_{MCU}) and protects against cell death in an in vivo ischemia-reperfusion (IR) injury model by preventing the activation of the mitochondrial permeability transition pore (MPTP). In addition, we found that *Mcu*-null mice lacked in vivo contractile responsiveness to β-adrenergic receptor (βAR) stimulation and in parallel were unable to activate mitochondrial dehydrogenases and meet energetic demand. Further experimental analysis confirmed a lack of energetic responsiveness to acute sympathetic stress, supporting the hypothesis that the physiological function of the MCU is to match Ca^{2+}-dependent contractile demands with mitochondrial metabolism during the "fight-or-flight" response.

RESULTS

Generation of a *Mcu* Conditional Knockout Mouse Model and Validation of Functionality

The *Mcu* targeting construct was designed with loxP sites flanking the critical exons 5–6, which encode the DIME motif, an evolutionarily conserved sequence hypothesized to be necessary for Ca^{2+} transport (Bick et al., 2012; Kwong et al., 2015, this issue). Three independent mutant ES cell lines were confirmed and subjected to morula aggregation and subsequent embryos transplanted into pseudo-pregnant females. Two of the three mutant ES cell lines produced germline mutant mice, which were crossed with ROSA26-FLPe mice for removal of the FRT-flanked neomycin cassette (Figure 1A). Cre-mediated deletion of exons 5–6 results in a frameshift and early termination of translation causing complete loss of MCU protein in all cells expressing Cre recombinase. Homozygous "floxed" mice ($Mcu^{fl/fl}$) were interbred, and mouse embryonic fibroblasts (MEFs) were isolated from E13.5 embryos. MEFs were infected with adenovirus expressing Cre recombinase (Ad-Cre) or βgal control virus and cells were lysed for western blot analysis of MCU protein expression 6 days later. Ad-Cre treatment resulted in a dose-dependent loss of MCU (Figure 1B). COXIV was used as a mitochondrial loading control. (Expression of additional $_{m}Ca^{2+}$ exchange associated proteins can be seen in (Figure S1A). ETC complex expression served as a mito loading control (Figure S1B). $Mcu^{fl/fl}$ Ad-Cre or Ad-βgal treated MEFs were subsequently infected with AAV-mitycam (mito-targeted genetic Ca^{2+} sensor) and cells imaged 48 hr later to monitor $_{m}Ca^{2+}$ exchange. ATP treatment (purinergic, IP3-mediated Ca^{2+} release) elicited a rapid decrease in mitycam fluorescent signal in $Mcu^{fl/fl}$ Ad-βgal MEFs (mitycam is an inverse reporter, data shown as $1\text{-}F/F_0$). Cells treated with Ad-Cre displayed almost complete loss of the acute $_{m}Ca^{2+}$ transient (Figure 1C). This difference was not attributable to a decrease in the $_{i}Ca^{2+}$ transient (Figure S1C). Quantification of mitycam amplitude immediately following ATP treatment found an ~75% decrease in $_{m}Ca^{2+}$ (Figure 1D). It should be noted that we did consistently observe that Mcu-KO MEFs continued to slowly take up Ca^{2+} and eventually reached levels equivalent to control cells. Next, $Mcu^{fl/fl}$ Ad-Cre- or Ad-βgal-infected MEFs were examined for $_{m}Ca^{2+}$ uptake capacity by loading digitonin permeabilized cells with the Ca^{2+} sensor, Fura-FF, and the membrane potential sensitive dye, JC-1 for simultaneous ratiometric recording. Cells were treated with thapsigargin to inhibit SERCA and block ER Ca^{2+} uptake. Upon reaching a steady-state membrane potential, cells were exposed to seven consecutive pulses of 5 μM Ca^{2+} (Figures 1E and 1F). A decrease in Fura signal after each bolus of bath Ca^{2+} represents $_{m}Ca^{2+}$ uptake. Quantitative analysis after exposure to 10 μM Ca^{2+} (a concentration where MCU is fully activated in non-excitable cells) revealed *Mcu*-null MEFs to have a near complete loss of $_{m}Ca^{2+}$ uptake compared to control MEFs (Figure 1G). Analysis of $\Delta\psi$ revealed no difference between groups at baseline or after delivery of 10 μM Ca^{2+}, confirming the observed change in uptake was not a result of an alteration in the driving force for $_{m}Ca^{2+}$ uptake (Figure 1H). Incremental increases in $_{m}Ca^{2+}$ eventually led to a decrease in membrane potential in βgal control MEFs, a phenomenon not observed in *Mcu*-null MEFs even after substantial Ca^{2+} challenge (Figure 1I). It should be noted that in an attempt to make a MEF $Mcu^{-/-}$ cell line, we crossed $Mcu^{fl/fl}$ mice with a transgenic germline-Cre model (B6.CMV-Cre, JAX Mice) to generate $Mcu^{+/-}$ for subsequent interbreeding. However, heterozygous mating (more than six litters) failed to yield $Mcu^{-/-}$ pups, suggesting homozygous deletion results in embryonic lethality.

Genetic Deletion of *Mcu* Results in the Complete Loss of Uniporter Ca^{2+} Uptake in ACMs

$Mcu^{fl/fl}$ mice were crossed with the well-characterized αMHC-Cre transgenic mouse model to yield cardiomyocyte-specific loss of *Mcu* (Figure 2A). Adult cardiomyocytes (ACMs) were isolated from wild-type (WT), αMHC-Cre, $Mcu^{fl/fl}$, and $Mcu^{fl/fl}$ × αMHC-Cre mice at 8–12 weeks of age. Western blot assessment found an ~80% reduction in MCU protein compared to all controls; in accordance with previous reports of the mosaicism of

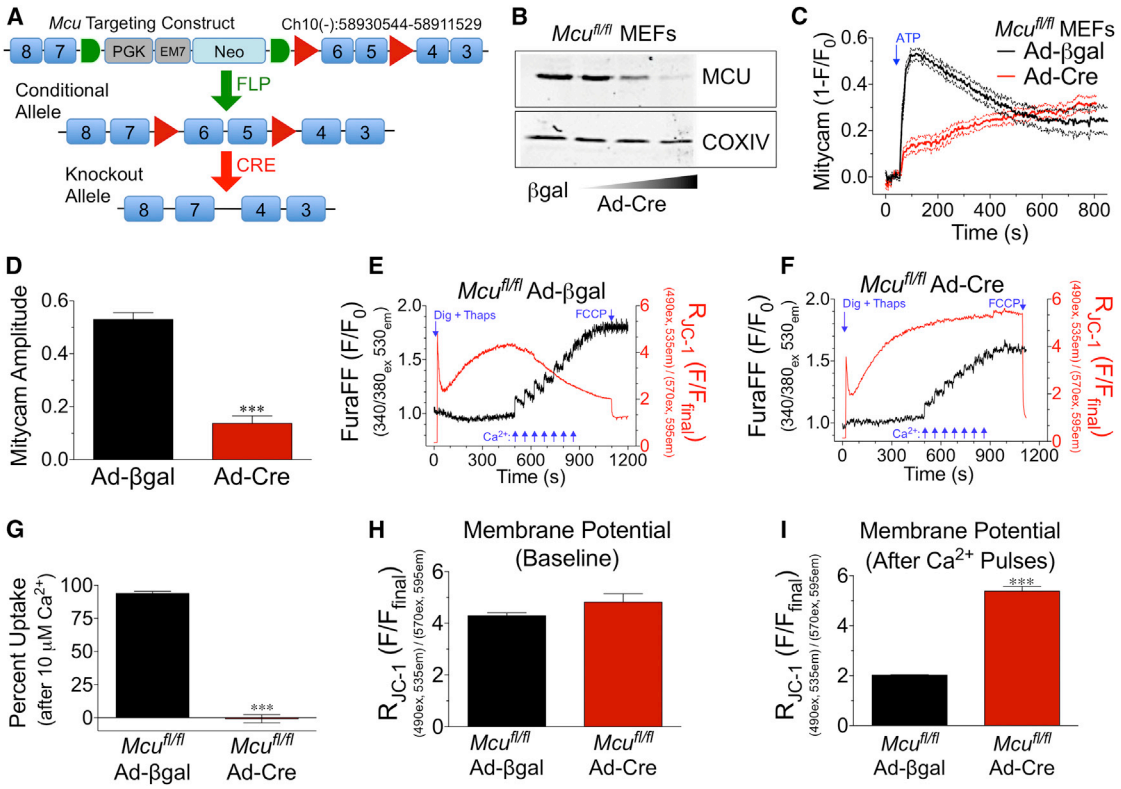

Figure 1. Generation of a Conditional Mcu Knockout Mouse Model and Confirmation of Functionality

(A) Schematic of *Mcu* targeting construct. LoxP sites (red triangles) flank exons 5–6. A neomycin (Neo) selection cassette is flanked by FRT sites (green half-circles). Mutant mice were crossed with ROSA26-FLPe mice for removal of Neo. Floxed mice (conditional allele) were crossed with cardiomyocyte-specific Cre recombinase driver lines resulting in deletion of *Mcu*.

(B) Mouse embryonic fibroblasts (MEFs) were isolated from $Mcu^{fl/fl}$ mice at E13.5. MEFs were infected with adenovirus expressing Cre recombinase (Ad-Cre) or the experimental control β-galactosidase (Ad-βgal). 6 days post-infection with Ad-Cre, cells were lysed and MCU protein expression was examined by western blot. COXIV was used as a mitochondrial loading control.

(C) $Mcu^{fl/fl}$ MEFs were treated with Ad-Cre or Ad-βgal and subsequently infected with Adeno encoding mitycam, $_{m}Ca^{2+}$ sensor, 48 hr prior to imaging. Baseline was recorded, and a single pulse of 1 mM ATP was delivered to liberate $_{i}Ca^{2+}$ stores.

(D) Signal means shown as solid lines with dashed lines displaying ± SEM $_{m}Ca^{2+}$ amplitude (peak intensity immediately after ATP – baseline).

(E) $Mcu^{fl/fl}$ MEFs were treated with Ad-βgal and loaded with the Ca^{2+} sensor (Fura-FF), and the Δψ sensor (JC-1) was permeabilized with digitonin and treated with thapsigargin (SERCA inhibitor) for simultaneous ratiometric monitoring during repetitive additions of 5 μM Ca^{2+} (blue arrows). FCCP was used as a control to collapse Δψ at the conclusion of each experiment.

(F) $Mcu^{fl/fl}$ MEFs were treated with Ad-Cre and subjected to identical experimental conditions.

(G) Percentage of $_{m}Ca^{2+}$ uptake versus Ad-βgal control cells following 10 μM Ca^{2+} (second pulse).

(H) JC-1-derived Δψ prior to Ca^{2+} additions.

(I) JC-1-derived Δψ following seven pulses of 5 μM Ca^{2+}.

All data shown as mean ± SEM, ***p<0.001 vs. βgal control.

the αMHC-Cre transgenic strain (Figure 2B) (Oka et al., 2006). No expression changes in ETC complex subunits were found (Figure S2A). To examine baseline $_{m}Ca^{2+}$ content, ACMs were loaded with the ratiometric Ca^{2+} reporter, Fura-2, and treated with Ru360 (MCU inhibitor), CGP37157 ($_{m}$NCX inhibitor), thapsigargin (SERCA inhibitor) and permeabilized with digitonin to block all Ca^{2+} flux. During spectrofluorometric recording the protonophore, FCCP, was injected to dissipate Δψ allowing the release of all matrix free-Ca^{2+} (Figure 2C). Quantification of these data by calibration of the Fura-2 reporter in our experimental system (Figure S2B) found no change in matrix Ca^{2+} content in *Mcu* knockout (KO) ACMs (Figure 2D). Next, $_{m}Ca^{2+}$ uptake capacity was evaluated in ACMs isolated from both $Mcu^{fl/fl}$ and $Mcu^{fl/fl}$ × αMHC-Cre mice (Figures 2E and 2F). The simultaneous recording of $_{m}Ca^{2+}$ uptake and membrane potential discovered that *Mcu KO* ACMs were completely refractory from high Ca^{2+} challenge and failed to take up Ca^{2+}, quantified after the second 10 μM Ca^{2+} pulse (Figure 2G). $Mcu^{fl/fl}$ × αMHC-Cre ACMs displayed a slightly higher baseline mitochondrial membrane potential, although not reaching statistical significance, confirming that the lack of Ca^{2+} uptake was not due to a decrease in Δψ (Figure 2H). Further, *Mcu*-null ACMs were entirely resistant to Ca^{2+}-overload loss of Δψ as observed in control cells. In fact, nine repeated boluses of 10 μM Ca^{2+} failed to elicit mitochondrial depolarization in *Mcu* KO ACMs (Figure 2I).

Please cite this article in press as: Luongo et al., The Mitochondrial Calcium Uniporter Matches Energetic Supply with Cardiac Workload during Stress and Modulates Permeability Transition, Cell Reports (2015), http://dx.doi.org/10.1016/j.celrep.2015.06.017

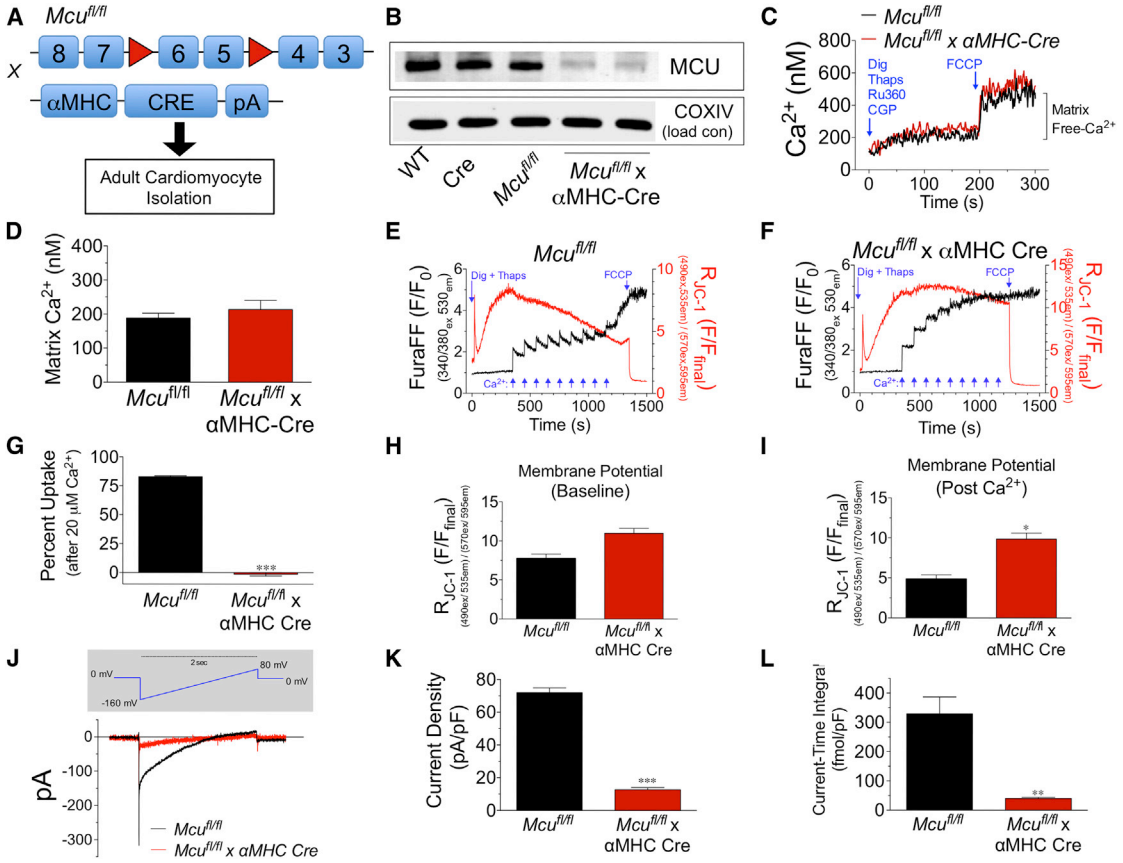

Figure 2. Biophysical Characterization of Mcu KO ACMs

(A) *Mcu*$^{fl/fl}$ mice were crossed with αMHC-Cre mice, and ACMs were isolated from hearts of adult mice.

(B) ACMs were isolated from wild-type (WT), αMHC-Cre (Cre), *Mcu*$^{fl/fl}$, *and Mcu*$^{fl/fl}$ × Cre. Samples were lysed and immunoblotted for MCU protein expression and the mitochondrial loading control COXIV.

(C) ACMs were loaded with the Ca^{2+} sensor Fura-2. The sarcolemma was permeabilized with digitonin in the presence of thapsigargin (SERCA inhibitor), CGP-37157 (mNCX inhibitor), and Ru360 (MCU inhibitor). Ca^{2+} levels were recorded and, upon reaching a stable baseline, free-$_mCa^{2+}$ was released from the mitochondrial matrix with FCCP.

(D) Quantification of matrix Ca^{2+} content after Fura calibration.

(E and F) *Mcu*$^{fl/fl}$ *or Mcu*$^{fl/fl}$ × αMHC-Cre ACMs were loaded with the Ca^{2+} sensor (Fura-FF), and the Δψ sensor (JC-1) was permeabilized with digitonin and treated with thapsigargin (SERCA inhibitor) for simultaneous ratiometric monitoring during repetitive additions of 10 μM Ca^{2+} (blue arrows). FCCP was used as a control to collapse Δψ at the conclusion of each experiment.

(G) Percentage of $_mCa^{2+}$ uptake versus *Mcu*$^{fl/fl}$ following the addition of 20 μM Ca^{2+}.

(H and I) JC-1 quantified Δψ at baseline and post-Ca^{2+} pulses.

(J) Mitochondria were isolated from ACMs, and mitoplasts were prepared to record MCU current (iMCU). Data are reported as mean current recordings; the voltage ramping protocol is above in gray shaded area.

(K) Current density measured in picoamperes per picofarad (pA/pF).

(L) Current-time integral measurements, femtomole per picofarad (fmol/pF).

Minimum of three independent experiments for all quantified data; all data shown as mean ± SEM, *p < 0.05, **p < 0.01, ***p < 0.001.

To confirm that deletion of the *Mcu* gene results in loss of MCU channel activity (I_{MCU}), we isolated ACMs, generated mitoplasts, and employed the whole-mitoplast voltage-clamping technique developed by the Clapham group that first established the uniporter as the prototypical uptake channel (Kirichok et al., 2004). I_{MCU} was absent in *Mcu*-null mitoplasts subjected to a ramping protocol from −160 mV to 80 mV (Figure 2J). Quantitative analysis revealed a decrease in current density (Figure 2K), and likewise the current-time integral (area under the curve) was minimal (Figure 2L). These data are in agreement with initial and subsequent reports of MCU channel biophysical activity (Chaudhuri et al., 2013; Fieni et al., 2012; Kirichok et al., 2004). Collectively, these experiments corroborate that *Mcu* is necessary for rapid $_mCa^{2+}$ uptake in cardiomyocytes.

MCU-Mediated $_mCa^{2+}$ Uptake Is a Significant Contributor to Myocardial IR Injury

Given the well-substantiated role of Ca^{2+} in activating the MPTP and the numerous reports that MPTP inhibition is a potent therapeutic strategy to reduce necrotic cell death (Rasola and

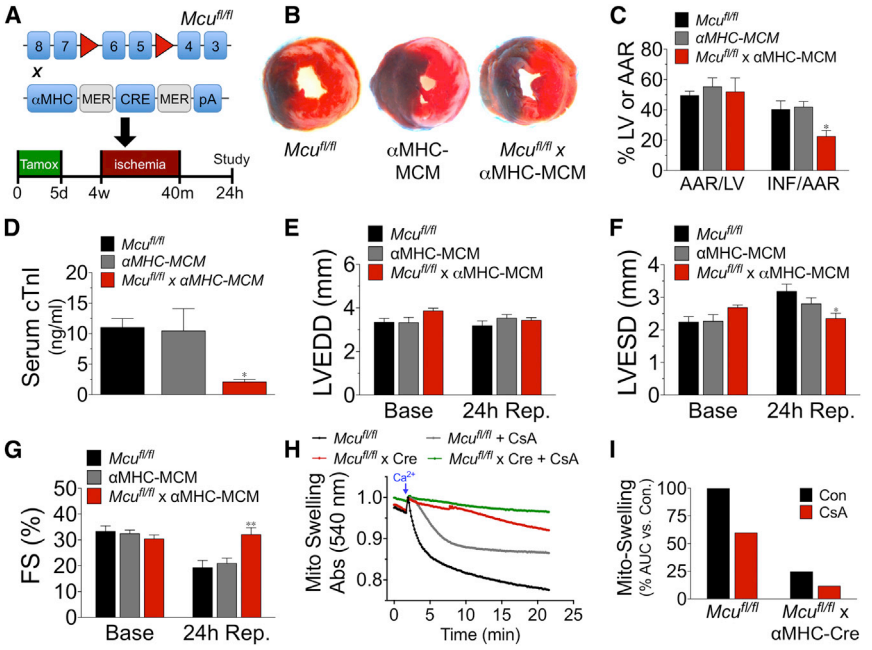

Figure 3. Genetic Ablation of *Mcu* Protects against Myocardial IR Injury

(A) *Mcu*$^{fl/fl}$, αMHC-Mer-Cre-Mer (αMHC MCM), and *Mcu*$^{fl/fl}$ × αMHC-Mer-Cre-Mer mice were treated with tamoxifen (40 mg/kg/day) for 5 days to induce cardiomyocyte-restricted Cre expression and allowed to rest for 3 weeks prior to 40 min of ischemia and 24-hr reperfusion.

(B) Representative mid-ventricular cross sections of TTC-stained hearts. (Evan's-blue-stained area, non-ischemic zone; remaining area, area-at-risk; white area, infracted tissue; red area, viable myocardium.)

(C) Planimetery analysis of infarct size by quantifying Evan's blue dye excluded area, area-at-risk (AAR), left ventricle (LV) area, and non-TTC-stained area = infarct (INF).

(D) 24 hr after reperfusion, serum was collected, and cardiac troponin-I (cTnI) was measured by ELISA.

(E–G) Mice were analyzed by echocardiography, and measurements of LV end-diastolic diameter (LVEDD), LV end-systolic diameter (LVESD), and percentage of fractional shortening (FS%) were acquired.

(H) Mitochondria were isolated from hearts of adult mice, and changes in swelling (decreased absorbance at 540 nm = increase in volume) were assessed ±2 μM CsA. Swelling was initiated by injection of 500 μM Ca^{2+}.

(I) Changes in swelling quantified by measuring the area under the curve (AUC) and correcting to control.

All in vivo experiments minimum of n = 7 for all groups; data shown as mean ± SEM, *p < 0.05, **p < 0.01.

Bernardi, 2011), we next assessed genetic loss of *Mcu* in an in vivo model of myocardial IR injury. *Mcu*$^{fl/fl}$, αMHC-MerCreMer (MCM), and *Mcu*$^{fl/fl}$ × αMHC-MCM (*Mcu* cKO) mice (aged 10–12 weeks) were all injected intraperitoneally (i.p.) for 5 consecutive days with 40 mg/kg tamoxifen (see Figures S3A and S3B for $_{m}Ca^{2+}$ exchange associated proteins and ETC complex expression post-tamoxifen) and 3 weeks later subjected to left coronary artery (LCA) ligation for 40-min and 24-hr reperfusion (Figure 3A). The evaluation of left ventricle (LV) infarct size by TTC staining and Evan's blue dye perfusion revealed *Mcu* cKO mice to have an ~45% reduction in infarct size (INF) per area at risk (AAR) versus controls; AAR was similar between all groups (Figures 3B and 3C). To corroborate this result, serum from the same cohort of mice was collected 24 hr after reperfusion, and a cardiac troponin-I (cTnI) ELISA was performed as a secondary marker of cardiomyocyte cell death. *Mcu*-deleted mice displayed an ~65% reduction in cTnI versus controls (Figure 3D). We also examined DNA fragmentation by TUNEL staining, to demarcate cell death. We found a significant reduction in TUNEL^{+} nuclei in the infarct boarder zone of *Mcu* cKO hearts as compared to controls (Figures S3C and S3D).

Echocardiographic assessment of LV function 24 hr post-IR revealed a significant preservation of LV end-systolic diameter (LVESD) and percentage of fractional shortening (FS%) in *Mcu* knockout mice (Figures 3E–3G). Additional M-mode echocardiographic data can be seen in Table S1. To account for differences in regional wall motion due to variances in infarct size, we utilized speckle-tracking of B-mode echocardiographic recordings and likewise found an improvement in LV function in *Mcu* cKO mice post-IR (Figures S3E–S3I).

To further examine the resistance of *Mcu*-null cardiomyocytes to mitochondrial depolarization during Ca^{2+} overload as reported above in Figure 2I, we next isolated mitochondria from hearts and employed the classical mitochondrial-swelling assay to examine MPTP opening. Mitochondria isolated from *Mcu*-KO hearts failed to swell in response to increasing bath Ca^{2+}, signified by a decrease in absorbance, in striking contrast to control mitochondria (Figure 3H, red versus black line). For these experiments, we utilized a substantial Ca^{2+} bolus (500 μM), such that the CypD inhibitor cyclosporine A (CsA) only had a partial inhibitory effect on swelling (gray line) in comparison to *Mcu* deletion. These data are quantified in Figure 3I as percentage of change in area under the curve versus control. It has previously been reported that MPTP opening occurs independent of CypD at high Ca^{2+} loads similar to those utilized here (Baines et al., 2005). To account for possible compensatory alterations in the expression of MPTP components, we immunoblotted for CypD, ANT, and VDAC (Figure S3J). We found no differences in expression between *Mcu* cKO and control hearts. These results support the hypothesis that the loss of *Mcu* prevents Ca^{2+} from entering the matrix and activating the MPTP and thereby reduces IR-mediated cardiomyocyte cell death.

$_{m}Ca^{2+}$ Uptake Is Necessary to Match Energetic Supply with β-Adrenergic Contractile Demand

Numerous studies have suggested that ECC Ca^{2+} cycling is integrated into mitochondria to match ATP production with workload (Williams et al., 2015). Given that we did not find a significant difference in baseline cardiac function or resting $_{m}Ca^{2+}$

Please cite this article in press as: Luongo et al., The Mitochondrial Calcium Uniporter Matches Energetic Supply with Cardiac Workload during Stress and Modulates Permeability Transition, Cell Reports (2015), http://dx.doi.org/10.1016/j.celrep.2015.06.017

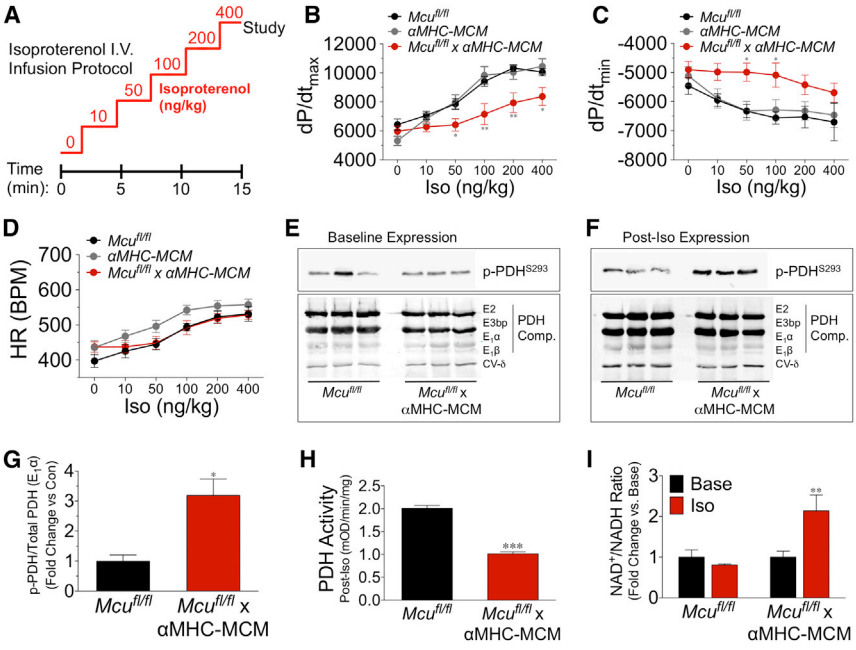

Figure 4. $_mCa^{2+}$ Uptake Is Required for β-Adrenergic-Mediated Increases in Contractility and Bioenergetic Responsiveness

(A) Mice in all groups received tamoxifen (40 mg/kg/day) for 5 days and 1 week later were subjected to an isoproterenol (Iso) infusion protocol (0.1–10 ng/ml) over 15 min.

(B–D) Invasive hemodynamic analysis of dp/dt_{max}, dp/dt_{min}, and heart rate (HR) during Iso infusion (minimum n = 7/group).

(E) Baseline expression analysis of pyruvate dehydrogenase (PDH) phosphorylation at S293 of the $E_1\alpha$ subunit and total PDH expression (subunits E2, E3bp, $E_1\alpha$, E1β). ETC Complex V-subunit δ was used as a loading control.

(F) Hearts were freeze-clamped at the conclusion of Iso infusion protocol and western blot examination of PDH phosphorylation at S293 of the $E_1\alpha$ subunit, and total PDH expression (subunits E2, E3bp, $E_1\alpha$, E1β) was performed.

(G) Fold change in PDH phosphorylation versus control. Band density analysis was calculated as $p\text{-PDH}^{S293}$/total PDH ($E_1\alpha$).

(H) PDH activity of samples from hearts during Iso administration, expressed as mOD/min/mg of tissue.

(I) Cardiac NAD^+/NADH ratio following Iso infusion; data were expressed as fold change versus baseline.

All data shown as mean ± SEM, *$p < 0.05$, **$p < 0.01$, ***$p < 0.001$.

content, we next induced acute cardiac stress using an adrenergic agonist to elevate the $_iCa^{2+}$ load in an attempt to unmask the physiological function of the MCU. *Mcu*$^{fl/fl}$, αMHC-MCM, and *Mcu* cKO mice were injected i.p. for 5 consecutive days with 40 mg/kg tamoxifen, and 10 days later we measured LV hemodynamic parameters during intravenous (i.v.) infusion of isoproterenol (Iso) (Figure 4A). *Mcu* cKO mice failed to increase LV contractility (dp/dt max) in response to β-adrenergic stimulation as compared to control mice (Figure 4B). In addition, there was a noted, although less dramatic, impairment in LV relaxation (dp/dt min, Figure 4C). There was no significant difference in heart rate (HR) between groups over the course of Iso infusion (Figure 4D).

Following 10 min of Iso infusion, we snap-froze ventricular tissue for metabolic analysis. We first evaluated the status of the pyruvate dehydrogenase complex (PDH), the prototypical $_mCa^{2+}$-dependent enzyme that converts pyruvate into acetyl-CoA for use in the tricarboxylic acid (TCA) cycle. PDH is a central component linking glycolysis to OxPhos and also a contributor to the NADH pool. $_mCa^{2+}$ is reported to increase PDH phosphatase activity (*PDP1*), which, in turn, dephosphorylates the S293 residue on the E1 subunit resulting in increased PDH enzymatic activity. There was no change in the baseline expression of phospho-PDH, total PDH complex (Figure 4E), or other proposed $_mCa^{2+}$-regulated dehydrogenases (α-ketoglutarate dehydrogenase and isocitrate dehydrogenase; Figure S4A). However, expression analysis of post-Iso samples revealed a substantial decrease in phosphorylation of S293-E1 in control hearts versus *Mcu* cKO samples (Figure 4F, top panel). There was no change in total protein expression for any of the PDH subunits post-Iso (Figure 4F, bottom panel). Quantification of phospho/total E1-PDH revealed *Mcu-KO* hearts to have greater than a 3-fold difference in phosphorylation versus controls, signifying a failure to activate PDH during adrenergic stimulation (Figure 4G). This result was confirmed by our observation of an ~50% decrease in Iso-stimulated PDH enzymatic activity in *Mcu* cKO hearts (Figures 4H and S4B). To examine baseline energetics in more detail and rule out any compensatory changes in our *Mcu* cKO model, we employed metabolomics to measure the levels of several prominent TCA intermediates (Figures S4C and S4D). Mass spectrometry of ventricular tissue found no difference in any of the metabolites assayed.

Next, we measured the NAD^+/NADH ratio, and, while we found no difference at baseline, acute Iso stimulation revealed an ~2-fold difference in *Mcu* cKO hearts versus controls (Figure 4I). We also examined the $NADP^+$/NADPH ratio and again found no difference at baseline but did find a trend of increased $NADP^+$/NADPH ratio in *Mcu* cKO hearts during Iso infusion (Figure S4E). This was somewhat surprising since we thought NADPH generation was primarily extra-mitochondrial via the pentose phosphate pathway. However, mitochondrial enzymes such as malic enzyme, NADP-linked isocitrate dehydrogenase, and mitochondrial methylenetetrahydrofolate dehydrogenase are other significant sources of NADPH production (Fan et al., 2014; Huang and Colman, 2005; Palmieri et al., 2015; Yang et al., 1996). It is intriguing to think that this may be another metabolic consequence of altering the $_mCa^{2+}$microdomain during stress, be it direct or indirect modulation.

To further examine the hypothesis that MCU-Ca^{2+} uptake is necessary to increase myocardial energy production in response to acute sympathetic signaling, we employed a cellular system to monitor energetic changes in real-time. ACMs were isolated

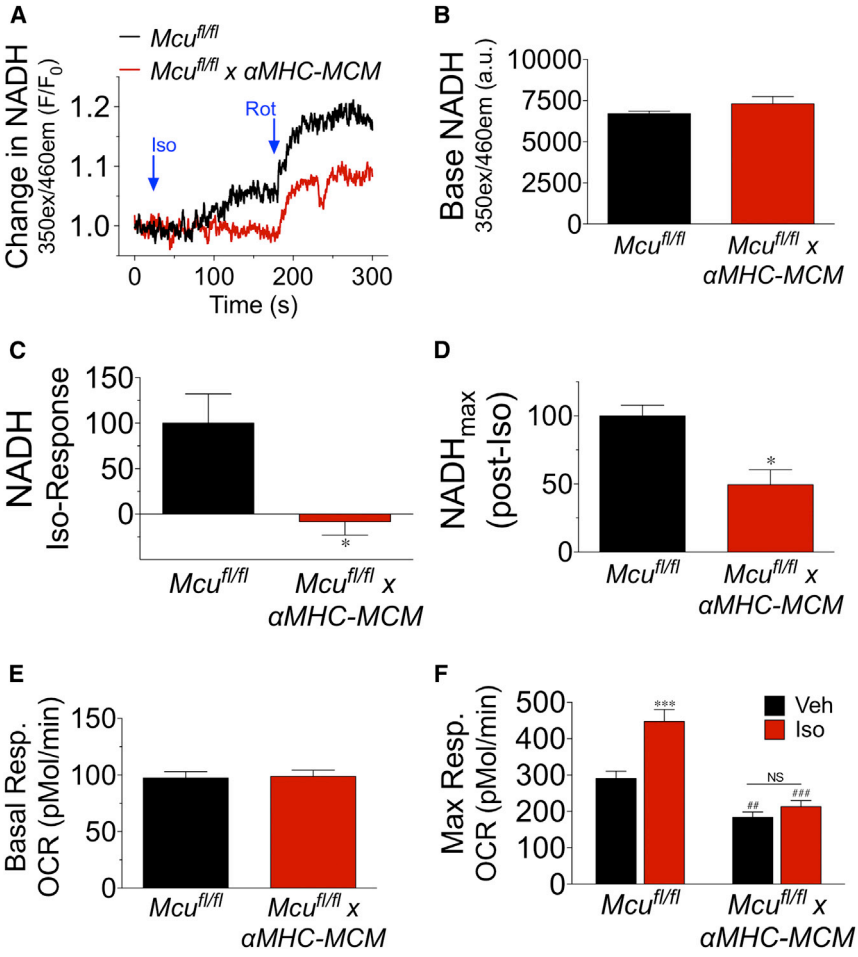

Figure 5. *Mcu* Is Necessary for β-Adrenergic Increases in Mitochondrial Energetics

ACMs were isolated from *Mcu*$^{fl/fl}$ and *Mcu*$^{fl/fl}$ × αMHC-MCM hearts 1 week post-tamoxifen treatment.

(A) ACMs were monitored spectrofluorometrically for changes in NADH autoflourescence after treatment with isoproterenol (Iso, 10 μM) followed by the addition of rotenone (Rot, 2 μM). Mean NADH recording from three independent experiments.

(B) Baseline NADH levels calculated as fluorescent intensity.

(C) Percentage of change in NADH levels following Iso treatment, corrected to *Mcu*$^{fl/fl}$ ACMs.

(D) NADH fluorescent intensity after treatment with rotenone, calculated as percentage of change from baseline to post-rotenone corrected to control ACMs.

(E) Isolated ACMs were assayed for mitochondrial OxPhos function using a Seahorse Bioanalyzer to measure the baseline oxygen consumption rate (OCR).

(F) ACMs were treated with either vehicle (Veh) or isoproterenol (Iso, 10 μM), and FCCP was injected to augment maximal OCR.

All data shown as mean ± SEM, $^{*}p < 0.05$, $^{***}p < 0.001$ versus Mcu$^{fl/fl}$; $^{\#\#}p < 0.01$, $^{\#\#\#}p < 0.001$ versus Veh.

from *Mcu*$^{fl/fl}$ and *Mcu*$^{fl/fl}$ × αMHC-MCM mice 10 days after administration of tamoxifen. We first monitored $_{i}Ca^{2+}$ transients at both baseline and during Iso delivery to rule out the possibility of decreased βAR responsiveness in our *Mcu* cKO cells (Figure S5). We found *Mcu* cKO ACMs to have no impairment in Iso-mediated augmentation of $_{i}Ca^{2+}$ signaling during pacing. Next, ACMs were monitored for changes in NADH autofluorescence intensity (Figure 5A). While we found no difference in basal NADH levels between groups (Figure 5B), the administration of Iso (10 μM) elicited a significant increase in NADH production in control ACMs, while *Mcu*-KO myocytes were unresponsive with NADH consumption being greater than production. Quantification of these data with correction to control ACMs can be seen in Figure 5C. To examine maximal NADH production in the presence of Iso, we next inhibited complex I of the ETC (NADH dehydrogenase) with rotenone. *Mcu*-KO ACMs displayed an ~50% reduction in maximal NADH production, as compared to control (Figure 5D). To evaluate whether the lack of NADH responsiveness correlated with an alteration in OxPhos capacity, we measured ACM oxygen consumption rates (OCR) using a Seahorse extracellular flux analyzer. Corroborating our previous data showing no change in baseline NADH, there was no difference in baseline respiration between groups (Figure 5E). Next, we examined maximal respiratory capacity ($_{max}$OCR, FCCP treatment) in the presence of Iso or vehicle (veh). *Mcu*-null ACMs displayed a significant reduction in $_{max}$OCR, as compared to controls, and were completely refractory to Iso-mediated increases in mitochondrial respiration (Figure 5F). In summation, these results support the concept of metabolic failure due to an inability to increase reducing equivalents during acute stress.

DISCUSSION

Since the 1970s, it has been apparent that mitochondria contained a protein capable of inducing an inward rectifying Ca^{2+} current (Sottocasa et al., 1972). The subsequent identification of a pharmacological inhibitor, of the channel, ruthenium red (RR), allowed investigators to begin to probe the cellular function of $_{m}Ca^{2+}$ exchange (Moore, 1971). Various studies employing RR or a derivative have implicated $_{m}Ca^{2+}$ in numerous cellular processes, most notably the regulation of metabolism, cell death, and buffering of cytosolic Ca^{2+} signaling (Hoppe, 2010). However, subsequent studies have found a multitude of cation channels that are inhibited by RR derivatives. Thus, off-target effects of these pharmacological agents may account for the conflicting results that have fueled the debate as to the true biological function of this microdomain. Further impeding causative experimentation was the unknown genetic identity of the constituents that comprise the $_{m}Ca^{2+}$ exchange machinery. Reports from two independent laboratories identified *MCU* as the channel-forming component of the MCU complex and documented its requirement for Ca^{2+} uptake (Baughman et al., 2011; De Stefani et al.,

Please cite this article in press as: Luongo et al., The Mitochondrial Calcium Uniporter Matches Energetic Supply with Cardiac Workload during Stress and Modulates Permeability Transition, Cell Reports (2015), http://dx.doi.org/10.1016/j.celrep.2015.06.017

2011). With this discovery, the race was on to generate a loss-of-function mouse model for comprehensive study to begin to put into context the vast and often controversial literature regarding how the dynamic flux of Ca^{2+} into and out of the mitochondrial matrix may regulate (patho)physiology. A recent report from Pan et al. details the phenotype of a *Mcu*-null mouse generated using a gene trap strategy (Pan et al., 2013). While the authors reported a complete loss acute $_{m}Ca^{2+}$ uptake in various cell types, the physiological results of the study were quite surprising. Perhaps most striking was that *Mcu* ablation had little effect on cardiac function, structure, or cell death. These results have prompted the field at large to question the relevance of cardiomyocyte $_{m}Ca^{2+}$ flux. Beyond this report, a number of other questions remained unresolved regarding the impact of $_{m}Ca^{2+}$ signaling in cardiomyocyte function.

Using a conditional knockout approach to specifically delete *Mcu* in cardiomyoyctes in adult mice coupled with in vivo experimental methodologies, we were able to document how acute $_{m}Ca^{2+}$ uptake impacts cardiac physiology. We found (1) a reduction in infarct size assessed both histologically by TTC staining and TUNEL and biochemically by cTnI levels coupled with in vivo LV functional data, that all support the notion that *Mcu*-mediated $_{m}Ca^{2+}$ uptake contributes to IR-induced cardiomyocyte cell death; (2) *Mcu* KO cells displayed a greater resistance to Ca^{2+} overload, capable of maintaining $\Delta\psi$ following numerous pulses of Ca^{2+} in contrast to control cells; and (3) cardiac mitochondria isolated from *Mcu*-null cardiomyocytes were completely resistant to swelling. Together these data suggest deletion of *Mcu* greatly decreases susceptibility to MPTP activation and thereby provides protection against necrotic cell death. This result is not surprising given the numerous reports implicating $_{m}Ca^{2+}$ load as a fundamental contributor to MPTP open probability (Rasola and Bernardi, 2011). Moreover, studies have shown that MPTP inhibition is potently cytoprotective, particularly in I/R injury, including a clinical trial evaluating the efficacy of cyclosporine-A (MPTP inhibitor) administration during reperfusion of the ischemic myocardium (Elrod and Molkentin, 2013; Piot et al., 2008). It is likely that MPTP inhibition was not the sole protective mechanism, as decreasing $_{m}Ca^{2+}$ load is also associated with decreased reactive oxygen species (ROS) generation during stress. Supporting this concept, we found a significant decrease in mitochondrial superoxide levels in *Mcu*-null cells following hypoxia/reoxygenation (Figures S1D and S1E).

However, our IR injury results are contradictory to those recently reported by Pan et al. (2013). Disparities in methodology likely account for the different results observed here. The previous study used a gene-trap approach with germline gene inactivation, versus our conditional, cardiomyocyte-specific deletion in the adult mouse. Therefore, compensatory pathways, induced by the loss of *Mcu* during development, may have allowed for the entry of Ca^{2+} into the matrix in sufficient quantity, independent of MCU, to activate mitochondrial-dependent death pathways or alternatively mitochondrial-independent cell-death pathways may be upregulated in this mouse. Our finding that germline deletion of *Mcu* in our model system was embryonically lethal, while knocking out *Mcu* after birth or in adulthood resulted in no discernable baseline phenotype, supports the notion that significant gene changes must have occurred prenatally in their model to support viability. Further, it may be that deletion of *Mcu* in other cell types in the heart, such as fibroblasts and endothelial cells, actually magnified injury by reducing the $_{m}Ca^{2+}$-buffering capacity in non-myocytes and thereby masked the protective effect of loss of *Mcu* in cardiomyocytes. Supporting this concept, we found that *Mcu*-null MEFs displayed an increase in $_{i}Ca^{2+}$ transient amplitude following IP3R stimulation (Figure S1C). Yet another possible reason is the disparity in ischemic models. The Pan et al. study employed an ex vivo Langendorff global hypoxia model compared to our in vivo LCA ligation IR model. There are major differences between these methodologies, and, while unlikely, perhaps the ex vivo model somehow lessens the contribution of MCU-dependent Ca^{2+} uptake in cardiomyocyte death. Our data do fit with previous reports of ruthenium red derivatives (MCU inhibitors) providing protection against IR injury (Zhang et al., 2006; Zhao et al., 2013).

The other major difference from the Pan et al. study is that we found no change in resting $_{m}Ca^{2+}$ content in *Mcu*-null cells, in contrast to their finding of ~70% reduction in skeletal muscle $_{m}Ca^{2+}$. Our results suggest a MCU-independent mechanism of $_{m}Ca^{2+}$ uptake is a significant contributor to homeostatic $_{m}Ca^{2+}$ levels. We hypothesize that the threshold for MCU-mediated Ca^{2+} entry is not reached under homeostatic conditions in adult cardiomyocytes and that an alternative slow $_{m}Ca^{2+}$ uptake mechanism must play a significant role. Direct evidence that MCU-independent $_{m}Ca^{2+}$ uptake exists can be seen in our experiment examining real-time flux in MEFs (Figure 1C). Although we observed complete loss of the acute and rapid MCU-like $_{m}Ca^{2+}$ uptake, $_{m}Ca^{2+}$ content continued to slowly rise with sustained $_{i}Ca^{2+}$ load and eventually reached a level equivalent to WT cells. It is possible that the lower $_{m}Ca^{2+}$ content previously reported in Pan et al. can be explained by methodological differences. We discovered that the slightest perturbation in either extracellular or $_{i}Ca^{2+}$ stores in WT cells induced an increase in $_{m}Ca^{2+}$ loading. We found that any Ca^{2+} liberated during our experimental procedure, be it from mitochondrial isolation or SERCA inhibition, was immediately taken up by WT mitochondria in a *Mcu*-dependent fashion. Therefore such a perturbation elevates $_{m}Ca^{2+}$ content in control cells and may lead to a false interpretation of decreased content in *Mcu* KO cells. This phenomenon can be seen in Figure S2C where, in control cells after permeabilization and addition of thapsigargin, we see a decrease in the Fura ratio prior to FCCP treatment signifying $_{m}Ca^{2+}$ uptake, whereas in *Mcu*-deleted cells we observe a rise in extra-mitochondrial Ca^{2+} levels. The addition of the MCU inhibitor, Ru360, and $_{m}$NCX inhibitor, CGP37157, prior to experimentation alleviated this problem. Summarizing the first part of our study, in a clinically relevant model of IR injury, we provide evidence that *Mcu*-mediated Ca^{2+} uptake is a significant mechanism driving MPTP-mediated cardiomyocyte cell death and cardiac dysfunction. Further, we hypothesize that the $_{m}Ca^{2+}$ exchange system possess a great deal of plasticity and that alternative uptake mechanisms maintain matrix Ca^{2+} content during homeostasis. A more detailed examination of this phenomenon in future studies may aid the discovery of novel exchangers and pathways that account for the observed "slow $_{m}Ca^{2+}$ uptake."

The heart is an aerobic organ that must constantly match energy supply with demand. The contractile function of the normal

heart changes significantly during normal activities. This has led to the theory that $_{i}Ca^{2+}$ cycling is integrated with mitochondria on a beat-to-beat basis to match ATP production with contractile demand as a real-time regulator of oxidative metabolism (Glancy and Balaban, 2012). However, our current findings suggest that rapid MCU-dependent Ca^{2+} uptake is dispensable for homeostatic cardiac function, as ablating *Mcu* had little effect on baseline function for all measured indices, including little to no change in LV function, structure, and cellular energetics. We found cardiomyocyte resting $_{m}Ca^{2+}$ content to be ~200 nM, and we did not detect appreciable mitochondrial uptake until concentrations of ~8 μM were reached (control ACMs displayed only ~17% uptake in response to a 10-μM-Ca^{2+} load). Both of these values fit nicely within the range of previous studies examining cardiac MCU function that were recently summarized in eloquent fashion by Williams et al. (2013). These data also agree with recent work proposing MICU1 binds MCU to inhibit uptake until a given threshold or set point of Ca^{2+} is overcome (Csordás et al., 2013; Mallilankaraman et al., 2012). Since it is assumed global ECC $_{i}Ca^{2+}$ cycling does not reach such levels in the homeostatic beating heart, we hypothesize that a slow MCU-independent influx mechanism must account for homeostatic maintenance of matrix Ca^{2+}, aided by balanced $_{m}$NCX efflux rates. It should be noted that Ca^{2+} levels of this magnitude might occur in discrete microdomains where a sub-population of mitochondria are tethered in close proximity to SR/T-tubule junctions (Chen et al., 2012). There are a number of mechanisms that theoretically could contribute to a slow MCU-independent $_{m}Ca^{2+}$ uptake including: $_{mito}$RyR, LETM1 (H^{+}/Ca^{2+} exchanger), reverse-mode $_{m}$NCX, or an as of yet unknown exchanger(s) (Beutner et al., 2001; Jiang et al., 2009; Palty et al., 2010). Additional evidence supporting MCU-independent uptake can be seen in a recent biophysical report describing a second "RR-insensitive" voltage-dependent inward rectifying current (Michels et al., 2009). We hope that our future experiments will aid the identification of this MCU-independent uptake mechanism.

While our data do not support a significant role for the MCU in basal cardiac physiology, cardiomyocyte-specific deletion did result in a striking inability to increase contractile function in response to the classic β-agonist, isoproterenol. Since a study published by Howell and Duke in 1906, it has been appreciated that Ca^{2+} is required for the "augmenting influence of the sympathetic upon the heart" (Howell and Duke, 1906). Our understanding has continued to evolve over the last century, and the various molecular mechanisms of how βAR signaling regulates changes in excitation-contraction coupling (ECC) have been defined (Bers, 2008). Our data extend these pathways to include MCU-dependent Ca^{2+} uptake as a mechanism necessary to upregulate energetics to support increases in cardiac contractility during acute sympathetic stress. Catecholamine signaling as occurs with the fight-or-flight response, strenuous exercise, or in the failing heart, elicits a marked increase in $_{i}Ca^{2+}$ levels. Specifically, isoproterenol has been shown to dramatically increase peak $_{i}Ca^{2+}$ and SR Ca^{2+} load/release to levels sufficiently beyond those we show here are required for MCU-dependent uptake (Curran et al., 2007). This large increase in $_{i}Ca^{2+}$ is integrated into mitochondria to directly impact cellular energetics at multiple control points. $_{m}Ca^{2+}$ increases the activity of three matrix dehydrogenases that are rate-limiting in the tricarboxylic (TCA) cycle (Denton, 2009). Most notably, matrix Ca^{2+} has been shown to indirectly activate pyruvate dehydrogenase (PDH), which converts pyruvate to acetyl-CoA for entry into the TCA cycle and as such also links glycolysis with OxPhos (McCormack and England, 1983). We found a marked decrease in PDH E1 phosphorylation following Iso treatment in control cells, indicative of increased $_{m}Ca^{2+}$-dependent phosphatase activity and subsequent PDH enzymatic activation. In contrast, dephosphorylation of PDH was completely lacking in *Mcu*-KO hearts and PDH activity during isoproterenol administration was reduced by ~50%. In both in vivo and in vitro experiments, we discovered that loss of *Mcu* ablated Iso-mediated increases in NADH and OxPhos capacity. Generally, our metabolic findings are in agreement with Pan et al., which found similar alterations in skeletal muscle metabolism and work capacity in $Mcu^{-/-}$ mice subjected to starvation (Pan et al., 2013). Similarly, our study found no change in baseline metabolic function or metabolite levels. However, our finding that HR was not altered in *Mcu* cKO mice does differ from a recent report by the Anderson group where they reported that an MCU-dominant-negative mouse model lacked chronotropic responsiveness to β-adrenergic stimulation (Wu et al., 2015). This may be due to a difference in methodology, as we did not examine HR with implantable telemeters in conscious mice void of anesthesia. Overall, our model does support their hypothesis of MCU-mediated Ca^{2+} entry playing a significant role in the cardiac fight-or-flight response.

In summary, we show that the physiological function of MCU-mediated Ca^{2+} uptake in the heart is to augment mitochondrial energetic signaling to match ATP production with contractile demand during periods of acute adrenergic stress. In addition, our findings support a pathological role for MCU Ca^{2+} influx driving mitochondrial depolarization and cell death during IR injury. While much work remains to fully elucidate all the molecular constituents of the MCU complex and their mechanistic function, our current study provides a fundamental framework to aid our understanding of $_{m}Ca^{2+}$ uptake in health and disease.

EXPERIMENTAL PROCEDURES

Please see the Supplemental Information for detailed experimental procedures.

Generation of Mcu Conditional Knockout Mice

The gene targeting strategy in embryonic stem cells to generate the Mcu-loxP mice that we used here is described in Kwong et al. (2015). In short, a *Mcu* conditional knockout mouse by recombinant insertion of a targeting gene construct containing loxP sites flanking exons 5–6 of the *Mcu* gene (ch10: 58930544-58911529) in mouse ES cells. Three independent mutant ES cell lines were confirmed and subjected to morula aggregation, and subsequent embryos were transplanted into pseudo-pregnant females. Two of the three mutant ES cell lines produced germline mutant mice, which were crossed with ROSA26-FLPe knockin mice for removal of the FRT-flanked neomycin cassette. Resultant $Mcu^{fl/fl}$ mice were crossed with cardiac specific-Cre transgenic mice, αMHC-Cre, and αMHC-MCM, to generate cardiomyocyte-specific *Mcu* knockouts. B6.CMV-Cre transgenic mice (Jackson Laboratory, stock # 006054) were used for germline deletion. For temporal deletion of *Mcu* using the MCM model, $Mcu^{fl/fl}$, αMHC-MCM, and $Mcu^{fl/fl}$ × αMHC-MCM were injected with i.p. 40 mg/kg/day of tamoxifen for 5 consecutive days. For all experiments, mice were 10–14 weeks of age. All mutant lines were maintained on the C57/BL6 background, and all experiments involving

Please cite this article in press as: Luongo et al., The Mitochondrial Calcium Uniporter Matches Energetic Supply with Cardiac Workload during Stress and Modulates Permeability Transition, Cell Reports (2015), http://dx.doi.org/10.1016/j.celrep.2015.06.017

animals were approved by Temple University's IACUC and followed AAALAC guidelines.

Western Blot Analysis

All procedures were carried out as previously reported (Elrod et al., 2010).

Isolation of ACMs

ACMs were isolated from ventricular tissue as described previously (Zhou et al., 2000). All cells were used within 4 hr of isolation.

Evaluation of $_{m}Ca^{2+}$ Uptake and Content

To evaluate $_{m}Ca^{2+}$ content, permeabilized ACMs were treated with RU360 and CGP-37157 to inhibit $_{m}Ca^{2+}$ flux. Fura2 (Invitrogen) was added to monitor extra-mitochondrial Ca^{2+}. FCCP was added to uncouple the $\Delta\psi$ and release matrix free-Ca^{2+}. To measure $_{m}Ca^{2+}$ uptake capacity, ACMs were permeabilized and Fura-FF (Invitrogen) was added to monitor extra-mitochondrial Ca^{2+}. JC-1 (Enzo Life Sciences) was added to monitor $\Delta\psi$. Fluorescence signals for JC-1 and Fura were monitored on a PTI spectrofluorometer. All details are previously reported (Mallilankaraman et al., 2012).

Mitochondria Isolation and Swelling Assay

Hearts were excised from mice and mitochondria were isolated as reported (Frezza et al., 2007). For the swelling assay, mitochondria were diluted in assay buffer, and absorbance (abs) was recorded at 540 nm every 5 s. 500 μM $CaCl_2$ was injected to induce swelling ± 2 μM Cyclosporin A (CsA) (Elrod et al., 2010).

ACM $_{i}Ca^{2+}$ Transients

Isolated ACMs were loaded with Fluo-4 AM (Invitrogen) and placed in a 37°C heated chamber on an inverted microscope stage. ACMs were perfused with Tyrode's buffer and paced at 0.5 Hz. After baseline recordings, cells were perfused with Tyrode's containing 100 nM Iso. Ca^{2+} transients were analyzed using Clampfit software.

Mitoplast Patch-Clamp Analysis of MCU Current

Following mitochondrial isolation, mitoplasts were prepared for patch-clamp studies. I_{MCU} was recorded as previously described in detail (Kirichok et al., 2004).

Metabolic Assays

Metabolomic analyses were carried out by metabolite profiling of ventricular tissue by LC-MS/MS as described (Jain et al., 2012). NAD/NADH and NADP/NADPH ratios were quantified using luminescence assays (Promega). PDH activity was quantified using a fluorometric assay (Mitosciences). In vitro experiments of ACM NADH production was monitored by recording autofluorescence using a spectrofluorometer. A XF96 extracellular flux analyzer (Seahorse Biosciences) was employed to measure OCR in isolated ACMs.

LV Echocardiography and Hemodynamics

Transthoracic echocardiography of the LV was performed and analyzed on a Vevo 2100 imaging system as previously reported (Elrod et al., 2007). Invasive hemodynamic measurements in anesthetized mice was performed using a pressure catheter inserted into the right carotid artery and guided into the LV. Right jugular vein catheterization allowed delivery of Iso during recording.

Myocardial IR Injury

LCA ligation and reperfusion was performed as previously described in Gao et al. (2010). Infarct size was measured as previously reported (Elrod et al., 2007). Serum was collected from mice after 24 hr R to measure cTnI using the Life Diagnostics ELISA kit. A TUNEL detection kit (Roche) was used to label DNA fragmentation in the infarct border zone of fixed heart sections.

MEF Isolation

Embryos were collected from $Mcu^{fl/fl}$ mice at E13.5 and MEFs isolated as previously reported (Baines et al., 2005). MEFs were treated with Ad-Cre or Ad-βgal for 24 hr. 6-day post-infection cells were used for experiments.

$_{i}Ca^{2+}$ and $_{m}Ca^{2+}$ Flux in MEFs

MEFs were infected with AAV-mitycam to measure $_{m}Ca^{2+}$ exchange or loaded with the $_{i}Ca^{2+}$ indicator, Fluo4-FF. Data were collected every 3 s and analyzed on Zen software.

Hypoxia/Reoxygenation

MEFs were plated on 35-mm glass plates and, after culturing for 24 hr, loaded with 5 μM MitoSOX Red (Invitrogen). Cells were placed in ischemic medium for 1 hr, reoxygenated with Tyrode's buffer, and imaged 5 min later to evaluate mitochondrial superoxide production.

Statistics

All results are presented as mean ± SEM. Statistical analysis was performed using Prism 6.0 software (GraphPad). Where appropriate column analyses were performed using an unpaired, two-tailed t test (for two groups) or one-way ANOVA with Bonferroni correction (for groups of three or more). For grouped analyses, either multiple unpaired t test with correction for multiple comparisons using the Holm-Sidak method or, where appropriate, two-way ANOVA with Tukey post hoc analysis was performed. p values <0.05 were considered significant.

SUPPLEMENTAL INFORMATION

Supplemental Information includes Supplemental Experimental Procedures, five figures, and one table and can be found with this article online at http://dx.doi.org/10.1016/j.celrep.2015.06.017.

AUTHOR CONTRIBUTIONS

J.W.E. and T.S.L. wrote the manuscript; J.W.E., T.S.L., J.P.L., A.Y., X.Z., P.G., J.S., S.S., E.G., and M.J. performed experiments. J.W.E., S.R.H., W.J.K., J.Y.C., and M.M., provided experimental oversight. J.W.E. and T.S.L. designed experiments, and J.W.E., M.M., and S.R.H. interpreted data.

ACKNOWLEDGMENTS

The authors express thanks to Dr. Joseph Rabinowitz's lab for amplification of AAV-mitycam. This work was supported by grants to J.W.E. from the NIH/NHLBI (HL123966), AHA (14SDG18910041), and W.W. Smith Charitable Trust (H1301) and NIH/NIDA (P01 DA037830, PI: K. Khalili).

Received: March 6, 2015
Revised: May 8, 2015
Accepted: June 4, 2015
Published: June 25, 2015

REFERENCES

Baines, C.P., Kaiser, R.A., Purcell, N.H., Blair, N.S., Osinska, H., Hambleton, M.A., Brunskill, E.W., Sayen, M.R., Gottlieb, R.A., Dorn, G.W., et al. (2005). Loss of cyclophilin D reveals a critical role for mitochondrial permeability transition in cell death. Nature *434*, 658–662.

Baughman, J.M., Perocchi, F., Girgis, H.S., Plovanich, M., Belcher-Timme, C.A., Sancak, Y., Bao, X.R., Strittmatter, L., Goldberger, O., Bogorad, R.L., et al. (2011). Integrative genomics identifies MCU as an essential component of the mitochondrial calcium uniporter. Nature *476*, 341–345.

Bers, D.M. (2008). Calcium cycling and signaling in cardiac myocytes. Annu. Rev. Physiol. *70*, 23–49.

Beutner, G., Sharma, V.K., Giovannucci, D.R., Yule, D.I., and Sheu, S.S. (2001). Identification of a ryanodine receptor in rat heart mitochondria. J. Biol. Chem. *276*, 21482–21488.

Bick, A.G., Calvo, S.E., and Mootha, V.K. (2012). Evolutionary diversity of the mitochondrial calcium uniporter. Science *336*, 886.

Brandes, R., and Bers, D.M. (2002). Simultaneous measurements of mitochondrial NADH and Ca(2+) during increased work in intact rat heart trabeculae. Biophys. J. *83*, 587–604.

Chaudhuri, D., Sancak, Y., Mootha, V.K., and Clapham, D.E. (2013). MCU encodes the pore conducting mitochondrial calcium currents. eLife *2*, e00704.

Chen, Y., Csordás, G., Jowdy, C., Schneider, T.G., Csordás, N., Wang, W., Liu, Y., Kohlhaas, M., Meiser, M., Bergem, S., et al. (2012). Mitofusin 2-containing mitochondrial-reticular microdomains direct rapid cardiomyocyte bioenergetic responses via interorganelle Ca(2+) crosstalk. Circ. Res. *111*, 863–875.

Csordás, G., Golenár, T., Seifert, E.L., Kamer, K.J., Sancak, Y., Perocchi, F., Moffat, C., Weaver, D., de la Fuente Perez, S., Bogorad, R., et al. (2013). MICU1 controls both the threshold and cooperative activation of the mitochondrial Ca^{2+} uniporter. Cell Metab. *17*, 976–987.

Curran, J., Hinton, M.J., Ríos, E., Bers, D.M., and Shannon, T.R. (2007). Beta-adrenergic enhancement of sarcoplasmic reticulum calcium leak in cardiac myocytes is mediated by calcium/calmodulin-dependent protein kinase. Circ. Res. *100*, 391–398.

De Stefani, D., Raffaello, A., Teardo, E., Szabò, I., and Rizzuto, R. (2011). A forty-kilodalton protein of the inner membrane is the mitochondrial calcium uniporter. Nature *476*, 336–340.

Denton, R.M. (2009). Regulation of mitochondrial dehydrogenases by calcium ions. Biochim. Biophys. Acta *1787*, 1309–1316.

Drago, I., De Stefani, D., Rizzuto, R., and Pozzan, T. (2012). Mitochondrial Ca2+ uptake contributes to buffering cytoplasmic Ca2+ peaks in cardiomyocytes. Proc. Natl. Acad. Sci. USA *109*, 12986–12991.

Elrod, J.W., and Molkentin, J.D. (2013). Physiologic functions of cyclophilin D and the mitochondrial permeability transition pore. Circ. J. *77*, 1111–1122.

Elrod, J.W., Calvert, J.W., Morrison, J., Doeller, J.E., Kraus, D.W., Tao, L., Jiao, X., Scalia, R., Kiss, L., Szabo, C., et al. (2007). Hydrogen sulfide attenuates myocardial ischemia-reperfusion injury by preservation of mitochondrial function. Proc. Natl. Acad. Sci. USA *104*, 15560–15565.

Elrod, J.W., Wong, R., Mishra, S., Vagnozzi, R.J., Sakthievel, B., Goonasekera, S.A., Karch, J., Gabel, S., Farber, J., Force, T., et al. (2010). Cyclophilin D controls mitochondrial pore-dependent Ca(2+) exchange, metabolic flexibility, and propensity for heart failure in mice. J. Clin. Invest. *120*, 3680–3687.

Fan, J., Ye, J., Kamphorst, J.J., Shlomi, T., Thompson, C.B., and Rabinowitz, J.D. (2014). Quantitative flux analysis reveals folate-dependent NADPH production. Nature *510*, 298–302.

Fieni, F., Lee, S.B., Jan, Y.N., and Kirichok, Y. (2012). Activity of the mitochondrial calcium uniporter varies greatly between tissues. Nat. Commun. *3*, 1317.

Foo, R.S., Mani, K., and Kitsis, R.N. (2005). Death begets failure in the heart. J. Clin. Invest. *115*, 565–571.

Frezza, C., Cipolat, S., and Scorrano, L. (2007). Organelle isolation: functional mitochondria from mouse liver, muscle and cultured fibroblasts. Nat. Protoc. *2*, 287–295.

Gao, E., Lei, Y.H., Shang, X., Huang, Z.M., Zuo, L., Boucher, M., Fan, Q., Chuprun, J.K., Ma, X.L., and Koch, W.J. (2010). A novel and efficient model of coronary artery ligation and myocardial infarction in the mouse. Circ. Res. *107*, 1445–1453.

Glancy, B., and Balaban, R.S. (2012). Role of mitochondrial Ca2+ in the regulation of cellular energetics. Biochemistry *51*, 2959–2973.

Hoppe, U.C. (2010). Mitochondrial calcium channels. FEBS Lett. *584*, 1975–1981.

Howell, W.H., and Duke, W.W. (1906). Experiments on the isolated mammalian heart to show the relation of the inorganic salts to the action of the accelerator and inhibitory nerves. J. Physiol. *35*, 131–150.

Huang, Y.C., and Colman, R.F. (2005). Location of the coenzyme binding site in the porcine mitochondrial NADP-dependent isocitrate dehydrogenase. J. Biol. Chem. *280*, 30349–30353.

Jain, M., Nilsson, R., Sharma, S., Madhusudhan, N., Kitami, T., Souza, A.L., Kafri, R., Kirschner, M.W., Clish, C.B., and Mootha, V.K. (2012). Metabolite profiling identifies a key role for glycine in rapid cancer cell proliferation. Science *336*, 1040–1044.

Jiang, D., Zhao, L., and Clapham, D.E. (2009). Genome-wide RNAi screen identifies Letm1 as a mitochondrial Ca2+/H+ antiporter. Science *326*, 144–147.

Kirichok, Y., Krapivinsky, G., and Clapham, D.E. (2004). The mitochondrial calcium uniporter is a highly selective ion channel. Nature *427*, 360–364.

Kwong, J.Q., Lu, X., Correll, R.N., Schwanekamp, J.A., Vagnozzi, R.J., Sargent, M.A., York, A.J., Zhang, J., Bers, D.M., and Molkentin, J.D. (2015). The mitochondrial calcium uniporter selectively matches metabolic output to acute contractile stress in the heart. Cell Rep. *12*, Published online June 25, 2015. http://dx.doi.org/10.1016/j.celrep.2015.06.002.

Mallilankaraman, K., Doonan, P., Cárdenas, C., Chandramoorthy, H.C., Müller, M., Miller, R., Hoffman, N.E., Gandhirajan, R.K., Molgó, J., Birnbaum, M.J., et al. (2012). MICU1 is an essential gatekeeper for MCU-mediated mitochondrial Ca(2+) uptake that regulates cell survival. Cell *151*, 630–644.

McCormack, J.G., and England, P.J. (1983). Ruthenium Red inhibits the activation of pyruvate dehydrogenase caused by positive inotropic agents in the perfused rat heart. Biochem. J. *214*, 581–585.

Michels, G., Khan, I.F., Endres-Becker, J., Rottlaender, D., Herzig, S., Ruhparwar, A., Wahlers, T., and Hoppe, U.C. (2009). Regulation of the human cardiac mitochondrial Ca2+ uptake by 2 different voltage-gated Ca2+ channels. Circulation *119*, 2435–2443.

Moore, C.L. (1971). Specific inhibition of mitochondrial Ca++ transport by ruthenium red. Biochem. Biophys. Res. Commun. *42*, 298–305.

Oka, T., Maillet, M., Watt, A.J., Schwartz, R.J., Aronow, B.J., Duncan, S.A., and Molkentin, J.D. (2006). Cardiac-specific deletion of Gata4 reveals its requirement for hypertrophy, compensation, and myocyte viability. Circ. Res. *98*, 837–845.

Palmieri, E.M., Spera, I., Menga, A., Infantino, V., Porcelli, V., Iacobazzi, V., Pierri, C.L., Hooper, D.C., Palmieri, F., and Castegna, A. (2015). Acetylation of human mitochondrial citrate carrier modulates mitochondrial citrate/malate exchange activity to sustain NADPH production during macrophage activation. Biochim. Biophys. Acta *1847*, 729–738.

Palty, R., Silverman, W.F., Hershfinkel, M., Caporale, T., Sensi, S.L., Parnis, J., Nolte, C., Fishman, D., Shoshan-Barmatz, V., Herrmann, S., et al. (2010). NCLX is an essential component of mitochondrial Na+/Ca2+ exchange. Proc. Natl. Acad. Sci. USA *107*, 436–441.

Pan, X., Liu, J., Nguyen, T., Liu, C., Sun, J., Teng, Y., Fergusson, M.M., Rovira, I.I., Allen, M., Springer, D.A., et al. (2013). The physiological role of mitochondrial calcium revealed by mice lacking the mitochondrial calcium uniporter. Nat. Cell Biol. *15*, 1464–1472.

Piot, C., Croisille, P., Staat, P., Thibault, H., Rioufol, G., Mewton, N., Elbelghiti, R., Cung, T.T., Bonnefoy, E., Angoulvant, D., et al. (2008). Effect of cyclosporine on reperfusion injury in acute myocardial infarction. N. Engl. J. Med. *359*, 473–481.

Rasola, A., and Bernardi, P. (2011). Mitochondrial permeability transition in Ca(2+)-dependent apoptosis and necrosis. Cell Calcium *50*, 222–233.

Rizzuto, R., Pinton, P., Carrington, W., Fay, F.S., Fogarty, K.E., Lifshitz, L.M., Tuft, R.A., and Pozzan, T. (1998). Close contacts with the endoplasmic reticulum as determinants of mitochondrial Ca2+ responses. Science *280*, 1763–1766.

Sottocasa, G., Sandri, G., Panfili, E., De Bernard, B., Gazzotti, P., Vasington, F.D., and Carafoli, E. (1972). Isolation of a soluble Ca 2+ binding glycoprotein from ox liver mitochondria. Biochem. Biophys. Res. Commun. *47*, 808–813.

Unitt, J.F., McCormack, J.G., Reid, D., MacLachlan, L.K., and England, P.J. (1989). Direct evidence for a role of intramitochondrial Ca2+ in the regulation of oxidative phosphorylation in the stimulated rat heart. Studies using 31P n.m.r. and ruthenium red. Biochem. J. *262*, 293–301.

Williams, G.S., Boyman, L., Chikando, A.C., Khairallah, R.J., and Lederer, W.J. (2013). Mitochondrial calcium uptake. Proc. Natl. Acad. Sci. USA *110*, 10479–10486.

Please cite this article in press as: Luongo et al., The Mitochondrial Calcium Uniporter Matches Energetic Supply with Cardiac Workload during Stress and Modulates Permeability Transition, Cell Reports (2015), http://dx.doi.org/10.1016/j.celrep.2015.06.017

Williams, G.S., Boyman, L., and Lederer, W.J. (2015). Mitochondrial calcium and the regulation of metabolism in the heart. J. Mol. Cell. Cardiol. *78*, 35–45.

Wu, Y., Rasmussen, T.P., Koval, O.M., Joiner, M.L., Hall, D.D., Chen, B., Luczak, E.D., Wang, Q., Rokita, A.G., Wehrens, X.H., et al. (2015). The mitochondrial uniporter controls fight or flight heart rate increases. Nat. Commun. *6*, 6081.

Yang, L., Luo, H., Vinay, P., and Wu, J. (1996). Molecular cloning of the cDNA of mouse mitochondrial NADP-dependent isocitrate dehydrogenase and the expression of the gene during lymphocyte activation. J. Cell. Biochem. *60*, 400–410.

Zhang, S.Z., Gao, Q., Cao, C.M., Bruce, I.C., and Xia, Q. (2006). Involvement of the mitochondrial calcium uniporter in cardioprotection by ischemic preconditioning. Life Sci. *78*, 738–745.

Zhao, Q., Wang, S., Li, Y., Wang, P., Li, S., Guo, Y., and Yao, R. (2013). The role of the mitochondrial calcium uniporter in cerebral ischemia/reperfusion injury in rats involves regulation of mitochondrial energy metabolism. Mol Med Rep *7*, 1073–1080.

Zhou, Y.Y., Wang, S.Q., Zhu, W.Z., Chruscinski, A., Kobilka, B.K., Ziman, B., Wang, S., Lakatta, E.G., Cheng, H., and Xiao, R.P. (2000). Culture and adenoviral infection of adult mouse cardiac myocytes: methods for cellular genetic physiology. Am. J. Physiol. Heart Circ. Physiol. *279*, H429–H436.

Cell Reports

Supplemental Information

The Mitochondrial Calcium Uniporter Matches Energetic Supply with Cardiac Workload during Stress and Modulates Permeability Transition

Timothy S. Luongo, Jonathan P. Lambert, Ancai Yuan, Xueqian Zhang, Polina Gross,

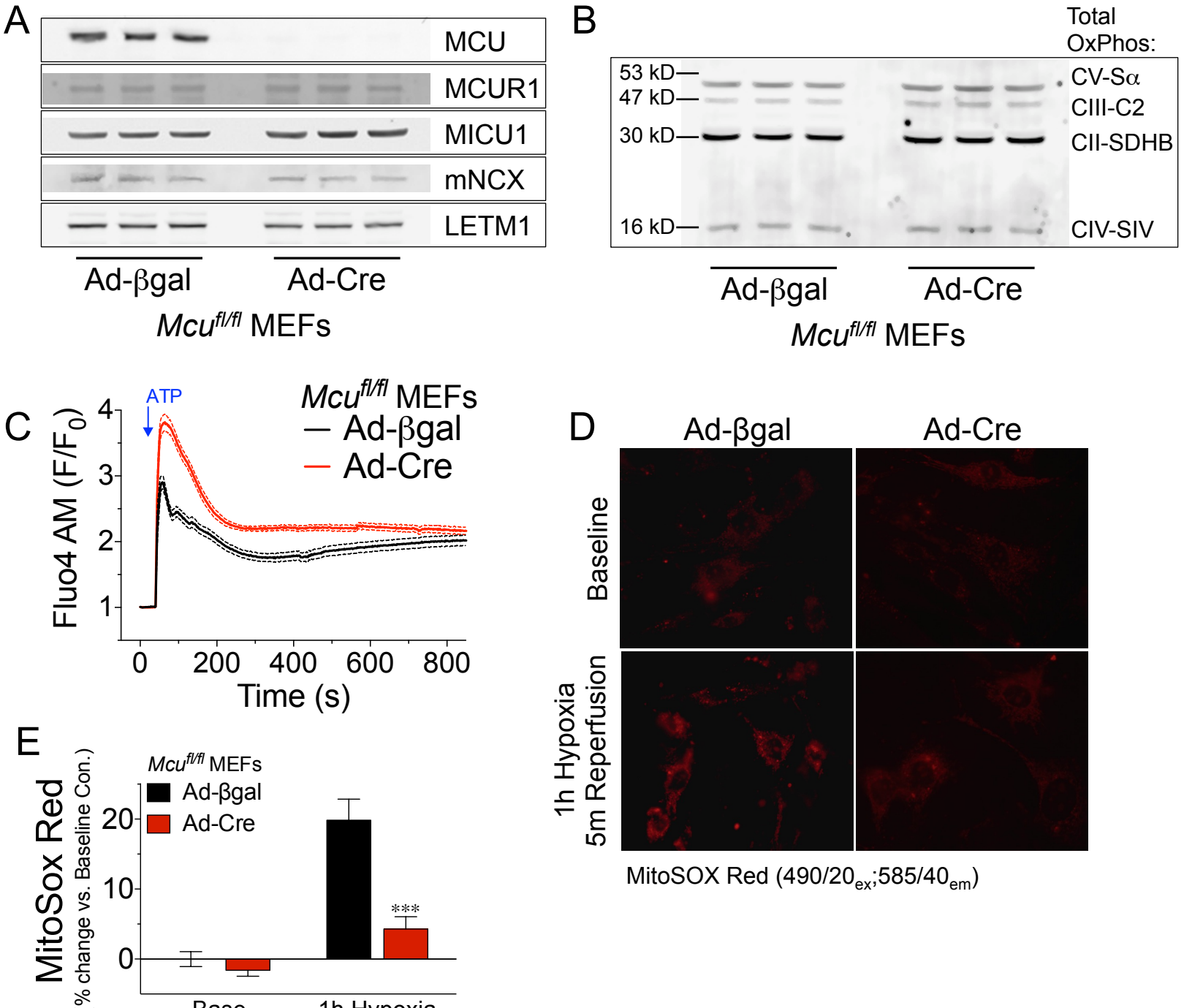
A
MCU
MCUR1
MICU1
mNCX
LETM1
Ad-βgal
Ad-Cre
Mcu fl/fl MEFs
B
Total OxPhos:
53 kD
47 kD
30 kD
16 kD
CV-Sα
CIII-C2
CII-SDHB
CIV-SIV
Ad-βgal
Ad-Cre
Mcu fl/fl MEFs
C
ATP
Mcu fl/fl MEFs
Ad-βgal
Ad-Cre
Fluo4 AM (F/F0)
Time (s)
D
Ad-βgal
Ad-Cre
Baseline
1h Hypoxia
5m Reperfusion
MitoSOX Red (490/20ex;585/40em)
E
MitoSox Red
(% change vs. Baseline Con.)
Mcu fl/fl MEFs
Ad-βgal
Ad-Cre
***
Base
1h Hypoxia
5m Reperfusion

FIGURE S1

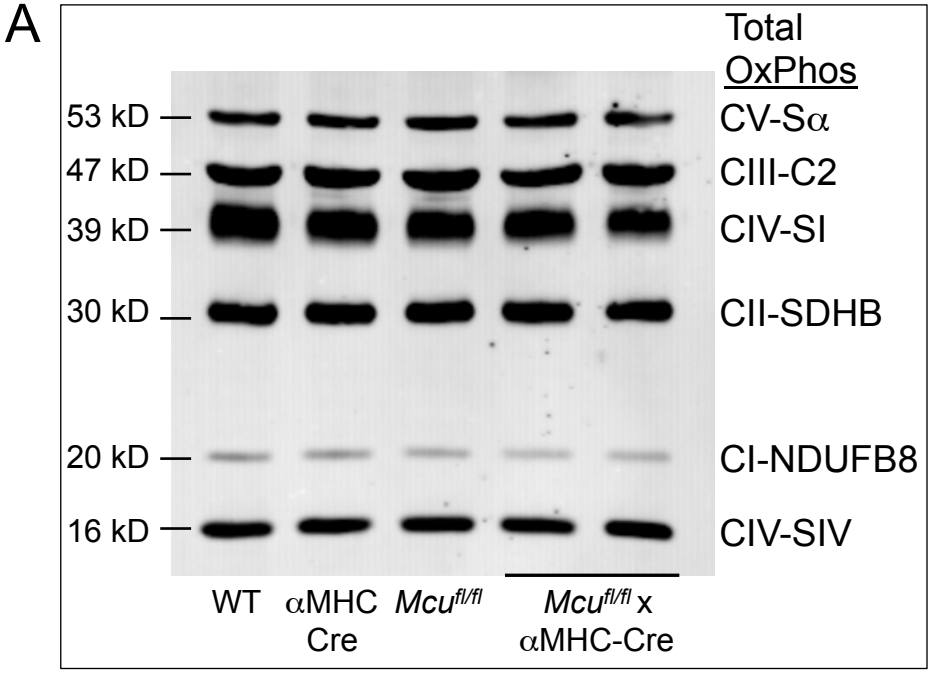
A
Total
OxPhos
53 kD
47 kD
39 kD
30 kD
20 kD
16 kD
CV-Sα
CIII-C2
CIV-SI
CII-SDHB
CI-NDUFB8
CIV-SIV
WT
αMHC Cre
Mcu fl/fl
Mcu fl/fl x αMHC-Cre

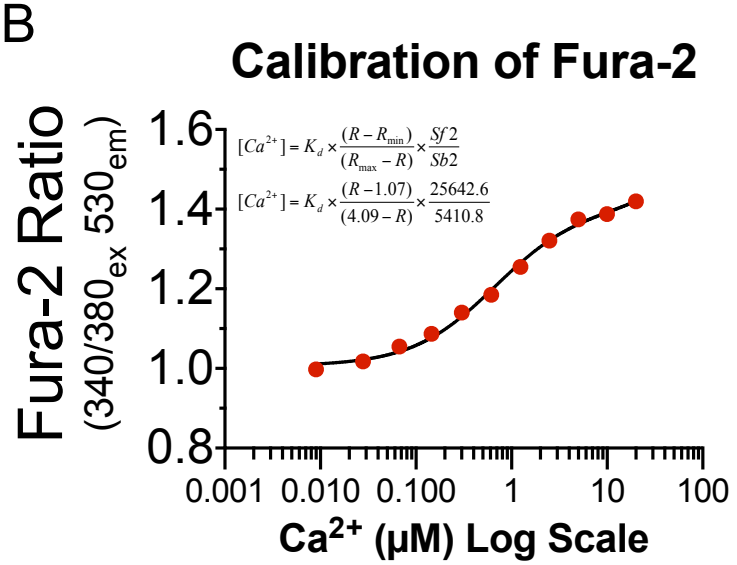
B
Calibration of Fura-2
Fura-2 Ratio (340/380ex 530em)
1.6
1.4
1.2
1.0
0.8
0.001
0.010
0.100
1
10
100
Ca2+ (μM) Log Scale

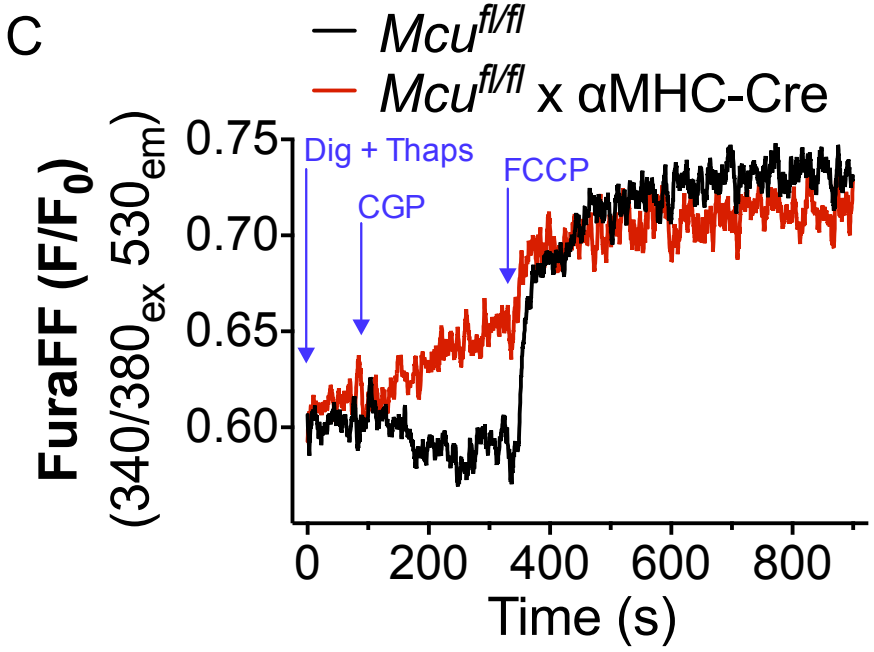
C
Mcu fl/fl
Mcu fl/fl x αMHC-Cre
FuraFF (F/F0) (340/380ex 530em)
0.75
0.70
0.65
0.60
Dig + Thaps
CGP
FCCP
0
200
400
600
800
Time (s)

FIGURE S2

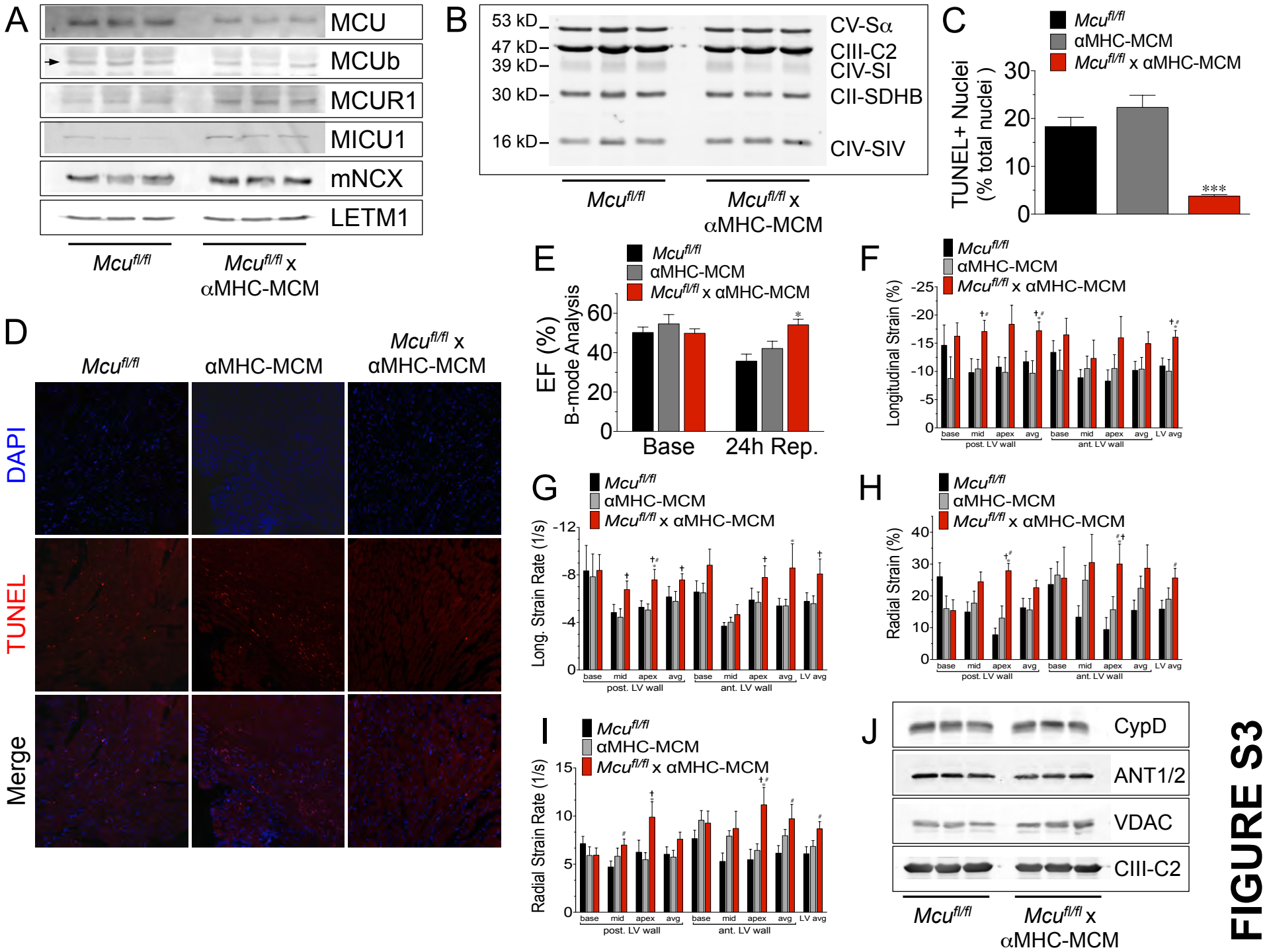
A
MCU
MCUb
MCUR1
MICU1
mNCX
LETM1
Mcu fl/fl
Mcu fl/fl x αMHC-MCM
B
53 kD
47 kD
39 kD
30 kD
16 kD
CV-Sα
CIII-C2
CIV-SI
CII-SDHB
CIV-SIV
Mcu fl/fl
Mcu fl/fl x αMHC-MCM
C
Mcu fl/fl
αMHC-MCM
Mcu fl/fl x αMHC-MCM
TUNEL+ Nuclei (% total nuclei)
***
D
Mcu fl/fl
αMHC-MCM
Mcu fl/fl x αMHC-MCM
DAPI
TUNEL
Merge
E
EF (%) B-mode Analysis
Base
24h Rep.
F
Longitudinal Strain (%)
base mid apex avg base mid apex avg LV avg
post. LV wall
ant. LV wall
G
Long. Strain Rate (1/s)
H
Radial Strain (%)
I
Radial Strain Rate (1/s)
J
CypD
ANT1/2
VDAC
CIII-C2
Mcu fl/fl
Mcu fl/fl x αMHC-MCM

FIGURE S3

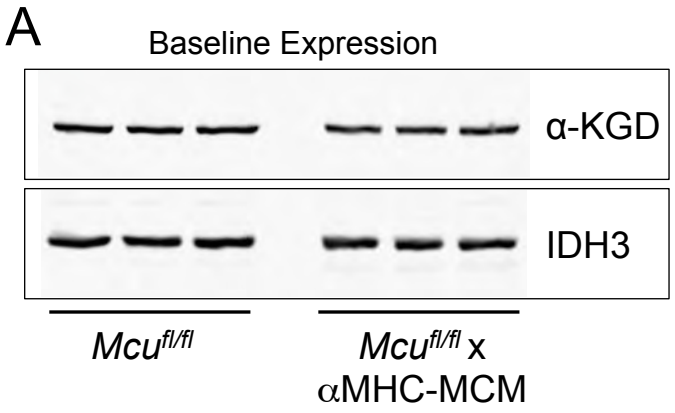
A
Baseline Expression
α-KGD
IDH3
Mcu^fl/fl
Mcu^fl/fl x αMHC-MCM

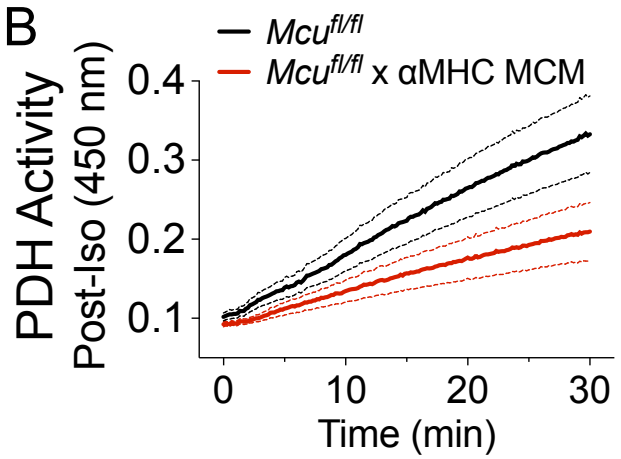
B
Mcu^fl/fl
Mcu^fl/fl x αMHC MCM
PDH Activity
Post-Iso (450 nm)
0.4
0.3
0.2
0.1
0
10
20
30
Time (min)

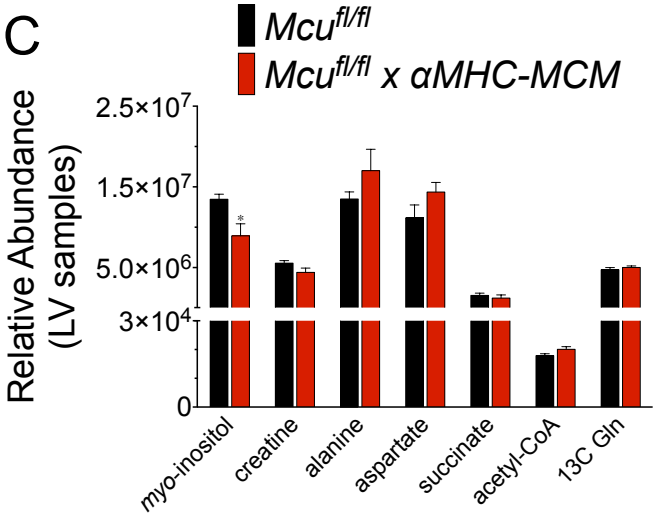
C
Mcu^fl/fl
Mcu^fl/fl x αMHC-MCM
Relative Abundance
(LV samples)
2.5×10^7
1.5×10^7
5.0×10^6
3×10^4
0
*
myo-inositol
creatine
alanine
aspartate
succinate
acetyl-CoA
13C Gln

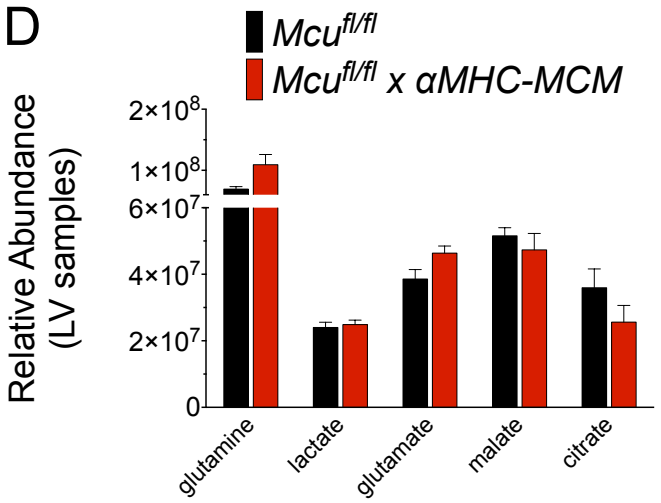
D
Mcu^fl/fl
Mcu^fl/fl x αMHC-MCM
Relative Abundance
(LV samples)
2×10^8
1×10^8
6×10^7
4×10^7
2×10^7
0
glutamine
lactate
glutamate
malate
citrate

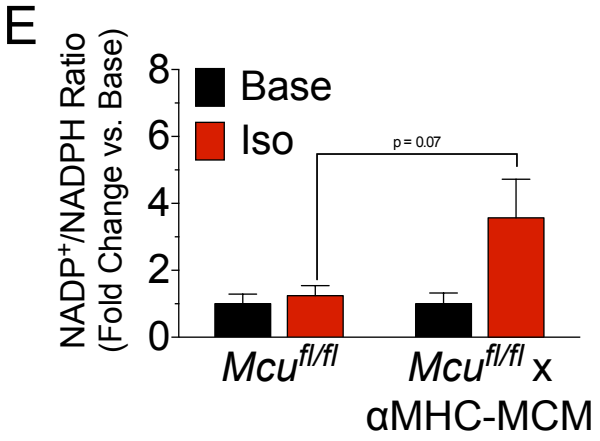
E
NADP+/NADPH Ratio
(Fold Change vs. Base)
Base
Iso
p = 0.07
8
6
4
2
0
Mcu^fl/fl
Mcu^fl/fl x
αMHC-MCM

FIGURE S4

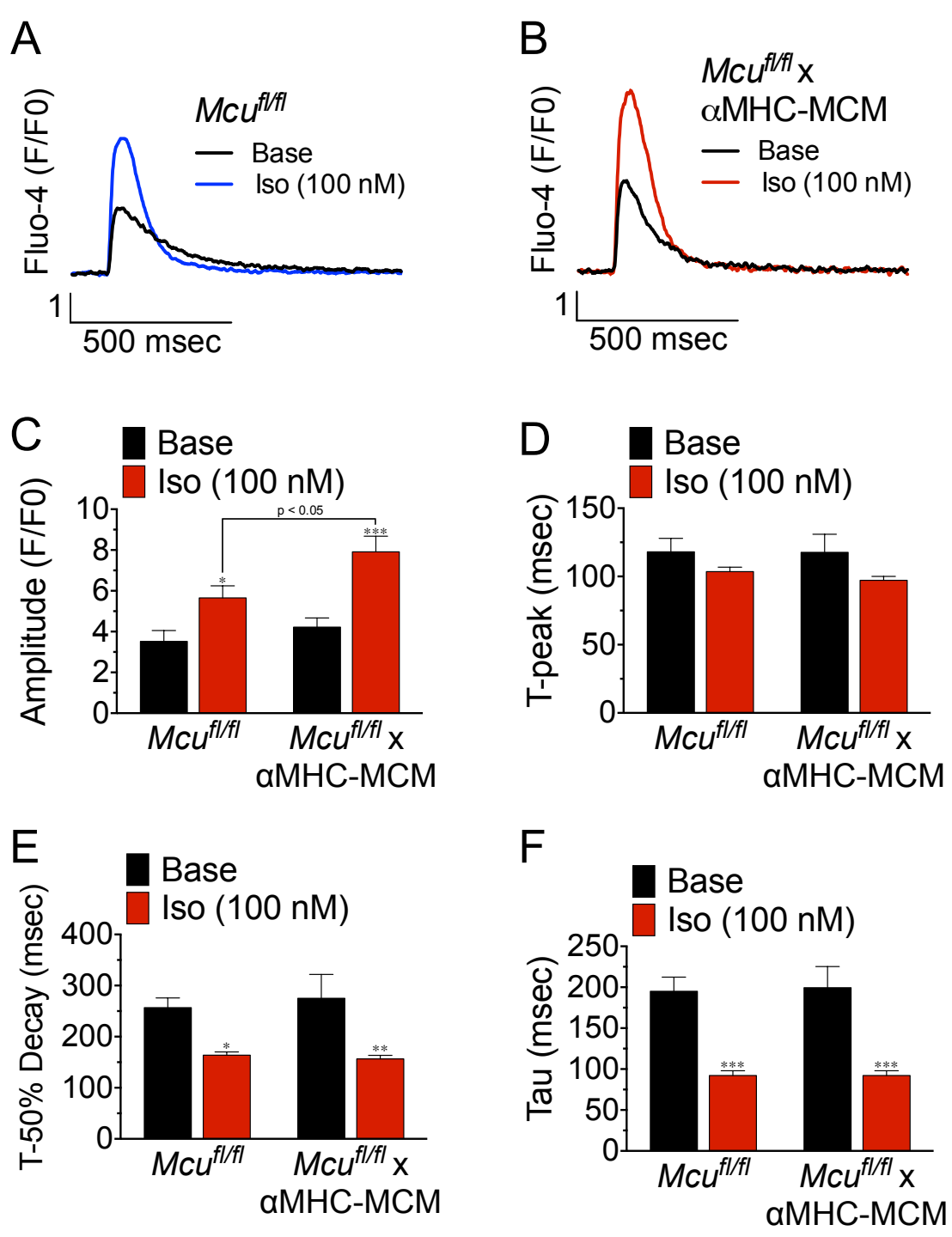
A
Mcu fl/fl
Base
Iso (100 nM)
Fluo-4 (F/F0)
1
500 msec
B
Mcu fl/fl x
αMHC-MCM
Base
Iso (100 nM)
Fluo-4 (F/F0)
1
500 msec
C
Base
Iso (100 nM)
p < 0.05
Amplitude (F/F0)
Mcu fl/fl
Mcu fl/fl x
αMHC-MCM
D
Base
Iso (100 nM)
T-peak (msec)
Mcu fl/fl
Mcu fl/fl x
αMHC-MCM
E
Base
Iso (100 nM)
T-50% Decay (msec)
Mcu fl/fl
Mcu fl/fl x
αMHC-MCM
F
Base
Iso (100 nM)
Tau (msec)
Mcu fl/fl
Mcu fl/fl x
αMHC-MCM

FIGURE S5

SUPPLEMENTAL FIGURE LEGENDS

Figure S1 – *related to Fig 1*. *Mcu* KO MEF $_{m}Ca^{2+}$ exchanger protein expression, $_{i}Ca^{2+}$ transients, and hypoxia/reoxygenation mediated mitochondrial superoxide production. MEFs were treated with Ad-Cre or Ad-βgal 6d prior to all experiments. **A**) Immunoblots for candidate MCU complex genes: MCU, MCUR1, and MICU1 and $_{mito}Ca^{2+}$ exchange proteins: mNCX and LETM1. **B**) Immunoblot of OxPhos complexes: Complex II succinate dehydrogenase subunit B (CII-SDHB) ~ 30kD, Complex III subunit Core 2 (CIII-C2) ~ 47kD, Complex IV subunit IV (CIV-SIV) ~ 16kD, ATP synthase subunit α (CV-Sα) ~ 53kD. **C**) Cytosolic Ca^{2+} transient after stimulation with 1-mM ATP using the Ca^{2+} sensor, Fluo4-AM. **D-E**) MEFs were loaded with MitoSOX Red (490/20ex; 585/40em) to evaluate mitochondrial superoxide production at baseline and after 1h hypoxia and 5min reperfusion. Mitochondrial superoxide production expressed as percent change vs. baseline of Ad-βgal. *(***p<0.001 vs. $Mcu^{fl/fl}$* Ad-βgal)

Figure S2 – *related to Fig 2*. Protein expression of ETC components, calibration of Fura-Ca^{2+} reporter, and $_{m}Ca^{2+}$ content recordings without pharmacologic MCU inhibition. **A**) Adult cardiomyocytes isolated from: wild-type (WT), αMHC-Cre (Cre), *$Mcu^{fl/fl}$, and $Mcu^{fl/fl}$* x Cre mice. Samples were lysed and subjected to western blot analysis for various OxPhos components including: Complex I subunit NDUFB8 (CI-NDUFB8) ~ 20kD, Complex II succinate dehydrogenase subunit B (CII-SDHB) ~ 30kD, Complex III subunit Core 2 (CIII-C2) ~ 47kD, Complex IV subunit I (CIV-SI) ~ 39kD, Complex IV subunit IV (CIV-SIV) ~ 16kD, ATP synthase subunit α (CV-Sα) ~ 53kD. **B**) Fura-2 was calibrated by the generation of a standard curve of Ca^{2+} (0.010 - 20 μM) in experimental intracellular buffer to quantify actual Ca^{2+} content as shown in Figure 2C. Fura-2 fluorescence ratio was converted to [Ca^{2+}] by the following equation: [Ca^{2+}] = Kd * (R-Rmin) / (Rmax - R) * Sf2 / Sb2 (Rmin = ratio in 0-Ca^{2+}, Rmax = ratio at saturation, Sf2 = 380/510 reading in 0-Ca^{2+}, Sb2 = 380/510 reading with Ca^{2+} saturation). **C**) ACMs were isolated and loaded with the Ca^{2+} sensor Fura-FF. The sarcolemma was permeabilized with digitonin in the presence of thapsigargin (SERCA inhibitor), CGP-37157 was added at 150s (mNCX inhibitor) and Ca^{2+} levels were recorded, and upon reaching a stable baseline, free-Ca^{2+} was released from the mitochondrial matrix with FCCP. It was observed that any Ca^{2+} liberated during our experimental procedure, such as SERCA inhibition, was immediately taken up by WT mitochondria (black trace) in a MCU-dependent fashion.

Figure S3 – *related to Fig 3*. Western blot assessment of MCU components, $_{m}Ca^{2+}$ exchangers, and ETC complexes following tamoxifen-mediated *Mcu* deletion, and TUNEL Staining 24h Post-I/R. *$Mcu^{fl/fl}$* and *$Mcu^{fl/fl}$* x αMHC-Mer-Cre-Mer (αMHC-MCM) mice were treated with tamoxifen (40 mg/kg/day) for 5d to delete *Mcu* and 1wk later examined for changes in protein expression. **A**) Immunoblots for candidate MCU complex genes: MCU, MCUb, MCUR1, MICU1 and $_{m}Ca^{2+}$ exchangers' mNCX and LETM1. **B**) Immunoblot of OxPhos complexes: Complex II succinate dehydrogenase subunit B (CII-SDHB) ~ 30kD, Complex III subunit Core 2 (CIII-C2) ~ 47kD, Complex IV subunit I (CIV-SI) ~ 39kD, Complex IV subunit IV (CIV-SIV) ~ 16kD, ATP synthase subunit α (CV-Sα) ~ 53kD. **C-D**) TUNEL Staining of paraffin-embedded heart sections 24h post-I/R, co-stained with DAPI and quantified as percent TUNEL positive nuclei vs. total nuclei in the infarct border zone. **E-I**) B-mode speckle-tracking analysis of LV function. **E**) Percent ejection fraction (EF%). **F**) Longitudinal Stain (%). **G**) Longitudinal Strain Rate (1/s). **H**) Radial strain (%). **I**) Radial Stain rate (1/s). **J**) Immunoblots of cyclophilin-D (CypD), adenine nucleotide translocator (ANT1/2), voltage-dependent anion channel (VDAC) and loading control complex-III C2 from *$Mcu^{fl/fl}$* and *$Mcu^{fl/fl}$* x αMHC-MCM ACMs. *(*p<0.05 vs.*

*$Mcu^{fl/fl}$ and αMHC-MCM, ***p<0.001 vs. $Mcu^{fl/fl}$ and αMHC-MCM $^{\#}$p<0.05 vs. $Mcu^{fl/fl}$, †p<0.05 vs. αMHC-MCM)*

Figure S4 – *related to Fig 4*. Quantification of LV metabolites, baseline expression of mitochondrial dehydrogenases, PDH activity rates, and $NADP^+$/NADPH ratio. A) Immunoblot of baseline expression of α-ketogluterate dehydrogenase (αKGD) and isocitrate dehydrogenase (IDH3). **B**) Traces of PDH activity from heart tissue post-isoproterenol administration (OD read at 450 nm). Dashed lines represent SEM. **C-D**) Mice 10wk of age were injected i.p. with 40mg/kg/d tamoxifien for 5d. 2wks later hearts were removed and snap-frozen in liquid nitrogen for LC-MS/MS metabolomic analysis. Relative abundance of various TCA metabolite levels. *(n=3 for all groups, *p<0.05 vs. $Mcu^{fl/fl}$).* **E**) $NADP^+$/NADPH ratio at baseline and post-isoproterenol represented as fold-change vs. baseline.

Figure S5 – *related to Fig 5*. Cytosolic Ca^{2+} transients in *Mcu* cKO isolated adult cardiomyocytes at baseline and following isoproterenol administration. ACMs were loaded with the cytosolic Ca^{2+} sensor, Fluo-4 AM and $_iCa^{2+}$ was examined during pacing at 0.5 Hz. **A**-**B**) Representative traces of $_iCa^{2+}$ transients at baseline and during Iso. **C**) Amplitude calculated as (F/F0). **D**) Time-to-peak of $_iCa^{2+}$ transients. **E**) Time-to-50% decay. **F**) Tau (rate of decay) of $_iCa^{2+}$ transients. *(*p<0.05 vs. $Mcu^{fl/fl}$, **p<0.01 vs. $Mcu^{fl/fl}$, ***p<0.001 vs. $Mcu^{fl/fl}$)*

Table S1 – *related to Fig 3*.

	Strain	n	IVS;d (mm)	IVS;s (mm)	LVID;d (mm)	LVID;s (mm)	LVPW;d (mm)	LVPW;s (mm)	EF (%)	FS (%)	LV Vol;d (µl)	LV Vol;s (µl)
Base	*Mcu*$^{fl/fl}$	9	0.88 ± 0.03	1.19 ± 0.03	3.34 ± 0.18	2.25 ± 0.16	0.99 ± 0.07	1.30 ± 0.07	62.3 ± 2.0	33.1 ± 2.1	47.3 ± 5.68	18.6 ± 3.14
	αMHC-MCM	8	0.95 ± 0.03	1.22 ± 0.05	3.33 ± 0.24	2.24 ± 0.20	0.94 ± 0.04	1.28 ± 0.07	61.9 ± 2.2	32.4 ± 1.4	47.5 ± 8.43	19.2 ± 4.28
	Mcu$^{fl/fl}$ x αMHC-MCM	8	0.89 ± 0.02	1.17 ± 0.05	3.82 ± 0.13	2.66 ± 0.08	0.83 ± 0.06	1.20 ± 0.08	57.8 ± 2.2	30.1 ± 1.5	63.5 ± 5.02	26.5 ± 2.03
24h Post-IR	*Mcu*$^{fl/fl}$	8	0.94 ± 0.03	1.14 ± 0.05	3.92 ± 0.17	3.18 ± 0.22	1.13 ± 0.16	1.38 ± 0.18	39.6 ± 5.6	19.2 ± 2.9	67.9 ± 6.68	42.2 ± 6.94
	αMHC-MCM	8	0.92 ± 0.04	1.19 ± 0.07	3.52 ± 0.17	2.80 ± 0.18	0.98 ± 0.06	1.14 ± 0.05	43.2 ± 3.7	20.9 ± 2.0	53.1 ± 6.19	31.0 ± 4.90
	Mcu$^{fl/fl}$ x αMHC-MCM	7	1.02 ± 0.13	1.39± 0.18	3.43 ± 0.43	2.35 ± 0.30*	0.86 ± 0.10	1.15 ± 0.13	60.7 ± 7.7**	32.0 ± 4.3**	49.0 ± 6.43	20.0 ± 3.24*

Table S1 – *related to Fig 3*. Echocardiographic results of left-ventricular (LV) function at baseline (base) and 24h post-IR. All values were collected from M-mode analyses to measure intraventricular septum thickness (IVS), left-ventricular interior dimensions (LVID), Left-ventricular posterior wall thickness (LVPW), left-ventricular volume (LV Vol) during diastole (d) and systole (s), percent ejection fraction (EF), and percent fractional shortening (FS). *(*p<0.05 vs. Mcu$^{fl/fl}$ and αMHC MCM)*

SUPPLEMENTAL EXPERIMENTAL PROCEDURES

Generation of Mcu conditional knockout mice*. Mcu* conditional knockout mice were generated in collaboration with the HHMI Gene Targeting & Transgenic Facility at the Janelia Research Campus. Insertion of a targeting construct containing loxP sites flanking exons 5 - 6 of the *Mcu* gene (ch10: 58930544-58911529) was performed in mouse ES cells. Three independent mutant ES cell lines were confirmed and subjected to morula aggregation and subsequent embryos transplanted into pseudo-pregnant females. Two of the three mutant ES cell lines produced germline mutant mice, which were crossed with ROSA26-FLPe knock-in mice for removal of the FRT-flanked neomycin cassette. Resultant $Mcu^{fl/fl}$ mice were crossed with cardiac specific-Cre transgenic mice, αMHC-Cre and αMHC-MCM, to generate cardiomyocyte-specific *Mcu* knockouts. B6.CMV-Cre transgenic mice (Jackson Laboratory, Stock # 006054) were used to attempt germline deletion. For temporal deletion of *Mcu* using the αMHC-MCM model, $Mcu^{fl/fl}$, αMHC-MCM, and $Mcu^{fl/fl}$ x αMHC-MCM were injected i.p. with 40 mg/kg/day of tamoxifien for 5 consecutive days. For all experiments mice were 10-14 wks of age. All mutant lines were maintained on the C57/BL6 background and all experiments involving animals were approved by Temple University's IACUC and followed AAALAC guidelines.

Western blot analysis*.* All tissue samples were lysed by homogenization in RIPA buffer. Samples were run by electrophoresis on 10% and 12% polyacrylamide Tris-glycine SDS gels. The following antibodies were used in the study: MCU, (1:1,000), Sigma-Aldrich; MCUb (1:1,000), Abgent; CCDC90A (MCUR1) (1:1,000), Abcam); MICU1 (1:500), Custom generation by Yenzyme, courtesy of the Madesh Lab; VDAC (1:2,500), Abcam; ANT (1:1,000), Santa Cruz Biotech; Cyclophilin D (1:5,000), Abcam; NCLX (mNCX) (1:1000), Santa Cruz N-12; LETM1 (1:1,000), Proteintech; ETC respiratory chain complexes (1:1,000), OxPhos Cocktail, Abcam; PDH subunits (1:1,000), Abcam; p-PDH^{S293} (1:1,000), Abcam; αKGD (1:250), Santa Cruz; IDH3 (1:500), Abcam; and Licor IR secondary antibodies (1:12,000). All images were acquired using a Licor Odyssey system. All procedures were carried out as previously reported (Elrod et al., 2010).

Isolation of adult mouse cardiomyocytes*.* Myocytes were isolated from ventricular tissue of mice as previously reported (Zhou et al., 2000). Briefly, mice were injected with heparin (1,500 U/kg) and anesthetized. Hearts were excised and the aorta was cannulated and perfused with a Ca^{2+}-free bicarbonate buffer (120-mM NaCl, 5.4-mM KCl, 1.2-mM $MgSO_4$, 1.2-mM NaH_2PO_4, 5.6-mM glucose, 20-mM NaHCO3, 10-mM 2,3-butanedione monoxime (BDM) and 5-mM taurine, gassed with 95% O2–5% CO2) at 37°C and then digested with collagenase B (1 mg/ml, Roche) supplemented with 0.05 mM Ca^{2+} and protease XIV (0.02 mg/ml, Sigma). Heart tissue was then cut into small pieces and aggregated by gentle pipetting to release the myocytes. Ca^{2+} was recovered with 10 min incremental additions (0.125-mM, 0.25-mM, 0.5-mM, 1-mM). Myocytes were then incubated at 37 °C with 5% CO_2. All cells were used within 3h of isolation.

Evaluation of $_mCa^{2+}$ uptake and content*.* To evaluate $_mCa^{2+}$ uptake and content, isolated adult cardiomyocytes were transferred to an intracellular-like medium containing (120-mM KCl, 10-mM NaCl, 1-mM KH_2PO_4, 20-mM HEPES-Tris), 3-μM thapsigargin, 80-μg/ml digitonin, protease inhibitors (Sigma EGTA-Free Cocktail), supplemented with 10-μM succinate and pH to 7.2. All solutions were cleared with Chelex 100 to remove trace Ca^{2+} (Sigma). For $_mCa^{2+}$ content: 150,000 digitonin permeabilized adult cardiomyocytes were treated with 1-μM Ru360 and 10-μM CGP-37157 to inhibit $_mCa^{2+}$ exchange. The myocytes were gently stirred and 1-μM Fura-2

(Invitrogen) was added to monitor extra-mitochondrial Ca^{2+}. Fluorescent signals were monitored in a spectrofluorometer (Delta RAM, Photon Technology Int.) at 340- and 380-nm ex/510-nm em. After acquiring baseline recordings, at 200s, 10-μM FCCP was added to uncouple the $\Delta\psi_m$ and release matrix free-Ca^{2+} (Miller et al., 2014).

To calibrate $_mCa^{2+}$ content, a standard curve of Ca^{2+} binding Fura-2 was generated from serial diluted Ca^{2+} standards (0.01 – 20 μM) in intracellular buffer. The Kd was calculated from the standard curve using Graphpad Prism 6.0 software. The fluorescence intensity was corrected to [Ca^{2+}] by the following equation: [Ca^{2+}] = Kd * (R-Rmin) / (Rmax - R) * Sf2 / Sb2 (Rmin=1.07, Rmax= 4.097, Sf2= 25642.6, Sb2= 5410.77).

To measure $_mCa^{2+}$ uptake capacity, 300,000 adult cardiomyocytes were gently stirred and 1 μM Fura-FF (Invitrogen) was added to monitor extra-mitochondrial Ca^{2+}. At 20s JC-1 (Enzo Life Sciences) was added to monitor $\Delta\psi_m$. Fluorescence signals were monitored at 490-nm excitation (ex)/535-nm emission (em) for the monomer, 570-nm ex/595-nm em for the J-aggregate of JC-1, and 340- and 380-nm ex/510-nm em for Fura-FF. Starting at 450 sec 10 μM Ca^{2+} boluses were added every 60 sec for 9 boluses. At 20s JC-1 was added to monitor Δψ. Fluorescence signals for JC-1 were monitored at 490ex/535 em for the monomer and 570ex/595em for the J-aggregate. Fura was monitored at 340/380ex and 510em. Starting at 450s 10 μM Ca^{2+} boluses were added every 60s. Clearance of extra-mitochondrial Ca^{2+} was representative of $_mCa^{2+}$ uptake. At completion of the experiment the protonophore, FCCP, was added. All experiments were conducted at 37 °C and recorded on a PTI spectrofluorometer. All details are previously reported (Mallilankaraman et al., 2012).

Mitochondria Isolation and Swelling. Hearts were excised from mice and mitochondria were isolated using a published protocol (Frezza et al., 2007). For the swelling assay, mitochondria were diluted in assay buffer containing (125-mM KCl, 20-mM HEPES, 2-mM $MgCl_2$, 2-mM K_2HPO_4 at pH 7.2) and supplemented with 10-mM succinate. Swelling was monitored using a Tecan Infinite M1000 Pro plate reader measuring absorbance at 540 ± 20 nm every 5 sec. A 500-μM $CaCl_2$ pulse was added to induce mitochondrial swelling +/- 2-μM Cyclosporin A (CsA) (i.e. decrease in absorbance) (Elrod et al., 2010).

***Adult mouse cardiomyocyte Ca^{2+} transient recordings*.** Isolated ACMs were loaded with 1-μM Fluo-4 AM (Invitrogen) and placed in a 37 °C heated chamber on an inverted microscope stage. Myocytes were perfused with a physiological Tyrode's buffer (150-mM NaCl, 5.4-mM KCl, 1.2 mM-$MgCl_2$, 10-mM glucose, 2-mM sodium pyruvate, and 5-mM HEPES, pH 7.4) containing 1-mM Ca^{2+}. Cells were paced at 0.5 Hz and Ca^{2+} transients continuously recorded and analyzed using Clampex10 software (Molecular Devices). After 2-3 min of baseline recording, 100-nM Isoproterenol (Sigma-Aldrich) was applied by changing the perfusion solution. After a stable baseline, 20 continuous Ca^{2+} transients were recorded and averaged for analysis. For intracellular Ca^{2+} fluorescence measurements, the F_0 was measured as the average fluorescence of the cell 100 ms prior to stimulation. The maximal Fluo-4 fluorescence (F) was measured for peak amplitude. Time to peak was calculated as the time from the beginning of the contraction to peak amplitude. Time to 50% decay was calculated as the time from the beginning of the contraction to 50% relaxation. Background fluorescence was subtracted from each experiment before measuring the peak intensity as F/F_0. Tau was measured as the decay rate of the Ca^{2+} transient.

Mitoplast patch-clamp analysis of MCU Current. Following mitochondria isolation from ventricular tissue, mitoplasts were prepared for patch-clamping (Kirichok et al., 2004). I_{MCU} was

recorded using a computer controlled Axon200B patch clamp amplifier with a Digidata 1320A acquisition board (pClamp 10.0 software; Axon Instruments). Mitoplasts were bathed in a solution containing (5-mM $CaCl_2$, 0.3-mM inorganic phosphate, 150-mM sodium gluconate, 5.4 mM-KCl, 10 mM-HEPES, pH 7.2). The pipette solution contained (150-mM sodium gluconate, 5 mM-NaCl, 135-mM sucrose, 10-mM HEPES, and 1.5-mM EGTA, pH 7.2). After formation of a giga-ohm seal (pipette resistance 20–35 mega-ohms), mitoplasts were ruptured with a 200-400mV pulse for a 2-6 ms duration. Mitoplast capacitance was measured (2.2–3.8 picofarads). After capacitance compensation, mitoplasts were held at 0 mV, and I_{MCU} was elicited with a voltage ramp (from −160 to +80 mV, 120 mV/s) as previously described in detail (Hoffman et al., 2013; Hoffman et al., 2014; Kirichok et al., 2004). All recordings were conducted at 30 °C.

Metabolic Assays. Metabolomic analyses were carried out by metabolite profiling of ventricular tissue by LC-MS/MS as described in Jain et al (Jain et al., 2012). To measure NAD^+/NADH and $NADP^+$/NADPH ratios hearts were lysed in PBS supplemented with protease and phosphatase inhibitors (Roche) prior to and after administration of isoproterenol. The ratios were evaluated using Promega NAD^+/NADH and $NADP^+$/NADPH Glo assays. Pyruvate dehydrogenase activity was quantified using the MitoSciences PDH activity assay on post-isoproterenol treated heart tissue. Activity was expressed as OD/min/mg of tissue.
To assess NADH production in isolated adult mouse cardiomyocytes, 150,000 adult cardiomyocytes were suspended in Tyrode's buffer (150-mM NaCl, 5.4-mM KCl, 5-mM HEPES, 10-mM glucose, 2-mM $CaCl_2$, 2-mM sodium pyruvate at pH 7.4) and NADH autofluorescence was read at 350ex/460em using a PTI spectrofluorometer. ACMs were gently stirred and 10-μM isoproterenol was added followed by 2-μM rotenone.
A Seahorse Bioscience XF96 extracellular flux analyzer was employed to measure adult cardiomyocyte oxygen consumption rates (OCR). 5,000 cardiomyocytes/well were plated in XF media pH 7.4 supplemented with 25-mM glucose and 1-mM sodium pyruvate. Basal OCR was measured +/- 10-μM isoproterenol then 1.5 μM FCCP was added to record maximal respiration. Detailed methodology is previously reported (Readnower et al., 2012).

Echocardiography. Trans-thoracic echocardiography of the LV was performed and analyzed on a Vevo 2100 imaging system (VisualSonics) as previously reported (Elrod et al., 2007). Mice were anesthetized with 2% isoflurane in 100% oxygen during acquisition. B-mode and M-mode images were collected in long- and short-axis. M-mode axis and B-mode strain analysis were performed using VisualSonics software for both short- and long-axis images.

Invasive hemodynamic measurements. Mice were anesthetized (avertin, 25 mg/kg) and a cutdown was performed and right carotid artery isolated for insertion of a 1.4-F pressure catheter (SPR-671, Millar Instruments) that was advanced into the LV. Right jugular vein catheterization allowed delivery of (0, 0.1, 0.5, 1, 5, 10 ng) isoproterenol during recording. All data was analyzed using Chart 6.0 software. All details have been previously reported (Elrod et al., 2007).

Myocardial IR-Injury. LCA ligation and reperfusion was performed as previously described in Gao et al. (Gao et al., 2010). Briefly, mice were anesthetized with isoflurane and the heart exposed via a left thoracotomy at the fifth intercostal space. A slipknot was tied around the left coronary artery (LCA) to enable ligation. The heart was returned to the chest cavity and the wound was sutured revealing the slipknot. After 40m ischemia, the slipknot was released and the ischemic area was allowed to reperfuse for 24h hours. To assess infarct size, after re-ligation of the LCA, hearts were injected with 3% Evan's Blue to delineate the area not-at-risk and 1mM heart sections were cut using a McIlwain Tissue Chopper. Heart sections were

incubated with 1% triphenyl tetrazolium chloride (TTC) for 5 min at 37 °C to demarcate viable tissue. Each slice was weighed and Image-J was used to quantify infarct area as previously reported (Elrod et al., 2007). Serum was isolated from mice 24h post-IR to measure cardiac troponin I (cTnI) using the Life Diagnostics, Inc. ELISA kit. Cell death was evaluated in the infarct border zone by TUNEL staining using the Roche In Situ Cell Death detection kit, TMR red. 4-5 images were taken per slide at 25x objective (TUNEL, 575/35ex and 632/60em; DAPI 360/40ex and 455/50em) and quantified by the percent of TUNEL positive nuclei verses DAPI positive nuclei.

MEF Isolation. Embryos were isolated from pregnant females at E13.5. The embryos were then decapitated and all the red organs removed. Next, tissue was minced up and digested in 0.25% trypsin supplemented with DNase for 10 min at 37°C. Digested tissue was then gently agitated by repeated pipetting to dissociate cells. Cells were then centrifuged at 1000 g for 5 min and the trypsin removed. The cell pellet was suspended in Dulbecco's Modified Eagle's Medium (DMEM) supplemented with 10% fetal bovine serum, non-essential amino acids, and penicillin/streptomycin in a 10 cm plate. Cells were then cultured and treated with Ad-Cre or Ad-βgal for 24h. 6d post-adenovirus treatment cells were used for experiments.

$_{i}Ca^{2+}$ and $_{m}Ca^{2+}$ flux in MEFs. MEFs were infected with AAV-mitycam to measure $_{m}Ca^{2+}$ exchange or loaded with the cytosolic Ca^{2+} indicator, 5-μM Fluo4-AM. Cells were imaged in Tyrode's buffer (150-mM NaCl, 5.4-mM KCl, 5-mM HEPES, 10-mM glucose, 2-mM $CaCl_2$, 2-mM sodium pyruvate at pH 7.4) on a Zeiss 510 confocal microscope using the 488 nm laser. Ca^{2+} flux was assessed in real-time, collecting data every 3s and analyzed on Zen software. $_{m}Ca^{2+}$ uptake capacity in non-excitable cells was evaluated similar to the detailed method provided above and as previously described (Mallilankaraman et al., 2012).

In Vitro Hypoxia/Reoxygenation. MEFs were plated onto 35mm glass plates and after culturing for 24h, loaded with 5 μM MitoSOX Red (Invitrogen). Cells were placed in ischemic medium (137-mM NaCl, 12-mM KCl, 4-mM HEPES, 0.49-mM $MgCl_2$, 0.9-mM CaCl2, 10-mM 2-deoxyglucose, 20-mM sodium lactate, 1-mM sodium dithionite at pH 6.5) for 1h and then reperfused in Tyrode's buffer and imaged 5min later (Punn et al., 2000). Cells were imaged (490/20ex; 585/40em) at baseline and 5m following reperfusion to evaluate mitochondrial superoxide production.

Statistics. All results are presented as mean and +/- SEM. Statistical analysis was performed using Prism 6.0 (Graph Pad Software). Where appropriate column analyses were performed using an unpaired, 2-tailed t-test (for 2 groups) or one-way ANOVA with Bonferroni correction (for groups of 3 or more). For grouped analyses either multiple unpaired t-test with correction for multiple comparisons using the Holm-Sidak method or where appropriate 2-way ANOVA with Tukey post-hoc analysis was performed. P values less than 0.05 were considered significant.

SUPPLEMENTAL REFERENCES

Elrod, J.W., Calvert, J.W., Morrison, J., Doeller, J.E., Kraus, D.W., Tao, L., Jiao, X., Scalia, R., Kiss, L., Szabo, C., et al. (2007). Hydrogen sulfide attenuates myocardial ischemia-reperfusion injury by preservation of mitochondrial function. Proceedings of the National Academy of Sciences of the United States of America *104*, 15560-15565.

Elrod, J.W., Wong, R., Mishra, S., Vagnozzi, R.J., Sakthievel, B., Goonasekera, S.A., Karch, J., Gabel, S., Farber, J., Force, T., et al. (2010). Cyclophilin D controls mitochondrial pore-dependent Ca(2+) exchange, metabolic flexibility, and propensity for heart failure in mice. J Clin Invest *120*, 3680-3687.

Frezza, C., Cipolat, S., and Scorrano, L. (2007). Organelle isolation: functional mitochondria from mouse liver, muscle and cultured fibroblasts. Nature protocols *2*, 287-295.

Gao, E., Lei, Y.H., Shang, X., Huang, Z.M., Zuo, L., Boucher, M., Fan, Q., Chuprun, J.K., Ma, X.L., and Koch, W.J. (2010). A novel and efficient model of coronary artery ligation and myocardial infarction in the mouse. Circulation research *107*, 1445-1453.

Hoffman, N.E., Chandramoorthy, H.C., Shamugapriya, S., Zhang, X., Rajan, S., Mallilankaraman, K., Gandhirajan, R.K., Vagnozzi, R.J., Ferrer, L.M., Sreekrishnanilayam, K., et al. (2013). MICU1 motifs define mitochondrial calcium uniporter binding and activity. Cell reports *5*, 1576-1588.

Hoffman, N.E., Chandramoorthy, H.C., Shanmughapriya, S., Zhang, X.Q., Vallem, S., Doonan, P.J., Malliankaraman, K., Guo, S., Rajan, S., Elrod, J.W., et al. (2014). SLC25A23 augments mitochondrial Ca(2)(+) uptake, interacts with MCU, and induces oxidative stress-mediated cell death. Molecular biology of the cell *25*, 936-947.

Jain, M., Nilsson, R., Sharma, S., Madhusudhan, N., Kitami, T., Souza, A.L., Kafri, R., Kirschner, M.W., Clish, C.B., and Mootha, V.K. (2012). Metabolite profiling identifies a key role for glycine in rapid cancer cell proliferation. Science (New York, N.Y *336*, 1040-1044.

Kirichok, Y., Krapivinsky, G., and Clapham, D.E. (2004). The mitochondrial calcium uniporter is a highly selective ion channel. Nature *427*, 360-364.

Mallilankaraman, K., Cardenas, C., Doonan, P.J., Chandramoorthy, H.C., Irrinki, K.M., Golenar, T., Csordas, G., Madireddi, P., Yang, J., Muller, M., et al. (2012). MCUR1 is an essential component of mitochondrial Ca(2+) uptake that regulates cellular metabolism. Nature cell biology *15*, 123.

Miller, B.A., Hoffman, N.E., Merali, S., Zhang, X.Q., Wang, J., Rajan, S., Shanmughapriya, S., Gao, E., Barrero, C.A., Mallilankaraman, K., et al. (2014). TRPM2 channels protect against cardiac ischemia-reperfusion injury: role of mitochondria. The Journal of biological chemistry *289*, 7615-7629.

Punn, A., Mockridge, J.W., Farooqui, S., Marber, M.S., and Heads, R.J. (2000). Sustained activation of p42/p44 mitogen-activated protein kinase during recovery from simulated ischaemia mediates adaptive cytoprotection in cardiomyocytes. The Biochemical journal *350 Pt 3*, 891-899.

Readnower, R.D., Brainard, R.E., Hill, B.G., and Jones, S.P. (2012). Standardized bioenergetic profiling of adult mouse cardiomyocytes. Physiological genomics *44*, 1208-1213.